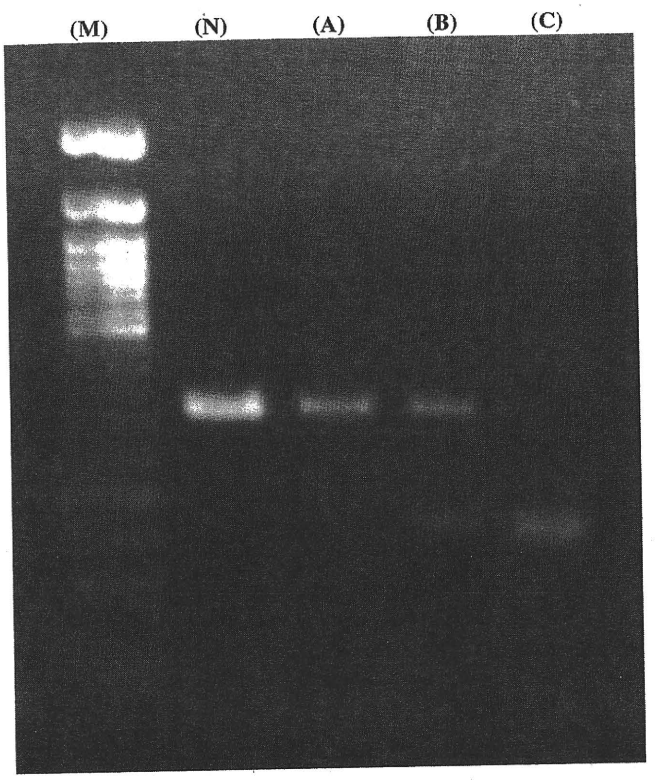

FIG. 1. Electrophoresed pattern of *NQO1* polymorphism. (**M**), marker; (**N**), no digestion (318 bp); (**A**), C/C genotype (318 bp); (**B**), C/T genotype (318 and 164 bp); (**C**), T/T genotype (164 bp). This figure shows the electrophoresed pattern of *NQO1* polymorphisms on 2% agarose gel stained with ethidium bromide. (**A**) This pattern was identified to be 318 bp for C/C wild type. (**B**) This pattern was identified to be a heterozygous type for C/T. (**C**) This pattern was identified to be a variant type for T/T. The *NQO1* T/T band genotype was expected to show two DNA bands of 164 bp and 154 bp; however, in this study, the T/T genotype resolved as a single band on agarose gel. The two bands were clearly resolved on a polyacrylamide gel.

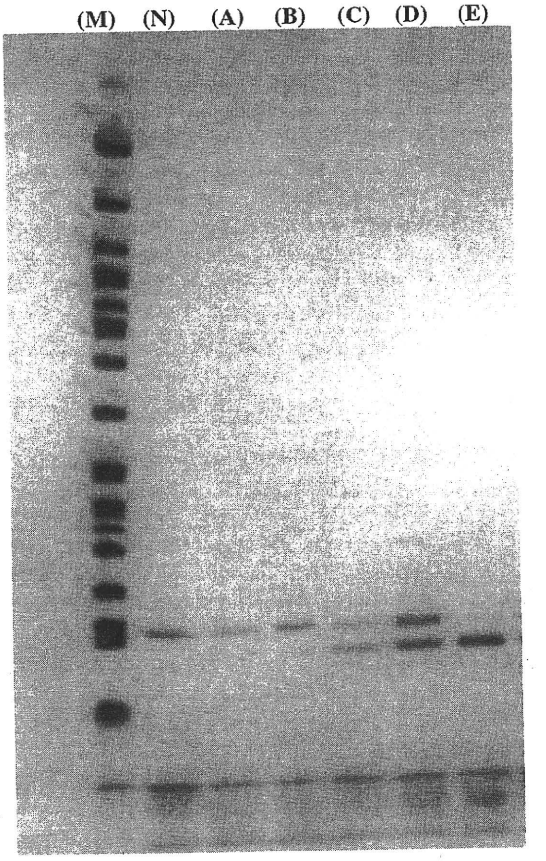

FIG. 2. Electrophoresed pattern of *SOD2* polymorphism on polyacrylamide gel. (**M**), marker; (**N**), no digestion (107 bp); (**A**) and (**B**), T/T genotype (107 bp); (**C**) and (**D**), C/T genotype (107 and 89 bp). (**E**), C/C genotype (89 bp). This figure showed the electrophoresed pattern of *SOD2* polymorphism on 12.5% polyacrylamide gel. (**A**) and (**B**) are patterns that were identified to be wild type for T/T. (**C**) and (**D**) are patterns that were identified to be a heterozygous type for C/T. (**E**) is a pattern that was identified to be a variant type for C/C. The band of 18 bp for C/T and C/C genotypes was not clearly identified because the band was very small; however, the 107 and 89 bp bands were clearly recognized on a polyacrylamide gel.

Results

NQO1 *and* SOD2 *polymorphism genotypes*

The allele frequencies of the *NQO1* and *SOD2* polymorphisms and the genotype frequencies are shown in Table 2. Three control samples could not be genotyped for the *SOD2* polymorphism. The genotype data were consistent with the Hardy–Weinberg equilibrium (*NQO1*—patient group: $\chi^2 = 2.79$, $p = 0.10$; control group: $\chi^2 = 0.01$, $p = 0.90$) (*SOD2*—patient group: $\chi^2 = 1.82$, $p = 0.18$; control group: $\chi^2 = 3.59$, $p = 0.06$). In the control group, the frequencies of the C/C, C/T, and T/T genotypes for the *NQO1* polymorphism were 39.2%, 46.4%, and 14.4%, respectively, whereas the frequencies of the C/C, C/T, and T/T genotype for the *SOD2* polymorphism were 0.8%, 34.4%, and 64.8%, respectively. In the UC patients, the genotype and allele frequencies of neither the *NQO1* nor the *SOD2* polymorphisms differed significantly from the controls.

Influence of NQO1 *and* SOD2 *polymorphisms on the clinical characteristics of UC*

We attempted to identify an association between the *NQO1* and *SOD2* polymorphisms and the clinical features of

TABLE 2. GENOTYPE FREQUENCY OF NAD(P)H:QUINONE OXIDOREDUCTASE 1 AND SUPEROXIDE DISMUTASE

	UC (n = 134)/ *control* (n = 125)	*OR (95% CI)*	p
NQO1			
C/C/ + C/T	109/107	1.00 (referent)	
T/T	25/18	0.73 (0.37–1.42)	0.354
SOD2			
C/C + C/T	39/44[a]	1.00 (referent)	
T/T	95/78	0.73 (0.43–1.24)	0.243

The genotype frequency of *NQO1* and *SOD2* is compared between UC and control. In the UC patients, the genotype and allele frequencies of neither the *NQO1* nor the *SOD2* polymorphisms differed significantly from the controls.

[a]Three control samples could not be genotyped for *SOD2* polymorphism.

OR, odds ratio; CI, confidence interval; *NQO1*, NAD(P)H:quinone oxidoreductase 1; *SOD2*, superoxide dismutase.

the UC patients (age of onset, sex, nature of clinical course, severity of colitis, and steroid resistance). The severity of colitis was classified using the Truelove and Witts' classification (Truelove *et al.*, 1978). We defined the steroid-resistant group as patients who did not have remission with a conventional steroid dose, and required surgery or other therapy, such as plasma exchange. The association between the clinical characteristics of the UC patients and the two polymorphisms are shown in Tables 3 and 4. Regarding the severity of colitis, more patients with the *NQO1* T/T genotype developed severe colitis compared to the other genotypes (odds ratio [OR] 2.20, 95% confidence interval [CI] 0.69–6.95). In Table 5, the data of steroid resistance in the UC patients and the two polymorphisms are summarized. A significantly greater number of patients with the *NQO1* T/T genotype showed steroid resistance than the other genotypes (OR 9.20, 95% CI 2.19–38.7, $p = 0.002$).

For the patients whose onset of UC was age 20 years or younger, more patients had the *SOD2* T/T genotype than the other genotypes (OR 6.56, 95% CI 0.83–51.7, $p = 0.074$). Considering the other factors investigated, such as the severity of colitis, there was no difference in the *SOD2* polymorphisms among the patients.

Discussion

In this study, we investigated the association between polymorphisms related to oxidative stress and UC. The *NQO1* gene is located on 16q22 (Jaiswal, 1991). The *NQO1* C609T polymorphism encoded by codon 187 in exon 6 (Traver *et al.*, 1997) includes a single C-to-T substitution of the *NQO1* cDNA that causes a Pro187Ser amino acid change. This substitution leads to a reduction in the activity of the enzyme C/T heterozygotes and no activity in T/T homozygotes (Siegel *et al.*, 1999). The T allele of *NQO1* may be associated with an increased risk of various type of malignancy, including leukemia (Larson *et al.*, 1999; Naoe *et al.*, 2000), esophageal cancer (Zhang *et al.*, 2003), and colorectal cancer (Lafuente *et al.*, 2000).

TABLE 3. CLINICAL FEATURES OF ULCERATIVE COLITIS AND NAD(P)H:QUINONE OXIDOREDUCTASE 1 POLYMORPHISM

Clinical feature	NQO1 *genotype* C/C+ C/T/T/T	*OR (95% CI)*	p
Age			
<20	12/3	1.00 (referent)	
≥20	97/22	0.89 (0.23–3.46)	0.871
Sex			
Male	65/12	1.00 (referent)	
Female	44/13	1.55 (0.65–3.72)	0.329
Extension			
Proctititis	21/2	0.57 (0.11–2.95)	0.499
Left-sided	45/14	1.83 (0.68–5.04)	0.228
Pancolitis	43/8	1.00 (referent)	
Type of clinical course			
First episode	11/5	1.00 (referent)	
Chronic relapse	67/12	0.38 (0.11–1.34)	
Chronic persistent	31/8	0.56 (0.15–2.17)	0.321
Severity			
Mild	34/6	1.00 (referent)	
Moderate	51/9	0.93 (0.32–3.10)	
Severe	24/10	2.20 (0.75–7.51)	0.203

The table shows the relationship between clinical features of UC and *NQO1* genotype. Regarding the severity of colitis, more patients with the *NQO1* T/T genotype developed severe colitis compared to the other genotypes (OR 2.20).

TABLE 4. CLINICAL FEATURES OF ULCERATIVE COLITIS AND SUPEROXIDE DISMUTASE POLYMORPHISM

Clinical feature	SOD2 *genotype* T/T/C/C+C/T	*OR (95% CI)*	p
Age			
<20	14/1	1.00 (referent)	
≥20	81/38	6.56 (0.83–51.7)	0.074
Sex			
Male	56/22	1.00 (referent)	
Female	39/17	1.09 (0.51–2.31)	0.826
Extension			
Proctititis	15/7	0.95 (0.32–2.78)	0.925
Left-sided	45/14	0.58 (0.25–1.33)	0.197
Pancolitis	34/18	1.00 (referent)	
Type of clinical course			
First episode	11/5	1.00 (referent)	
Chronic relapse	26/14	0.75 (0.23–2.45)	
Chronic persistent	58/20	1.19 (0.34–4.15)	0.746
Severity			
Mild	27/11	1.00 (referent)	
Moderate	46/14	0.72 (0.29–1.83)	
Severe	22/14	1.50 (0.57–3.99)	0.489

The table shows the relationship between clinical features of UC and *SOD2* genotype. For the patients whose onset of UC was age 20 years or younger, a higher proportion had the *SOD2* T/T genotype than the other genotypes (OR 6.56, $p = 0.074$).

TABLE 5. STEROID RESISTANCE WITH ULCERATIVE COLITIS AND TWO POLYMORPHISMS

Steroid resistance	*Genotype*	*OR (95% CI)*	p
NQO1	C/C+C/T/T/T		
Steroid effective ($n = 65$)	58/7	1.00 (referent)	
Steroid resistance ($n = 18$)	11/7	9.20 (2.19–38.7)	0.002
SOD2	T/T/C/C+C/T		
Steroid effective ($n = 65$)	44/21	1.00 (referent)	
Steroid resistance ($n = 17$)	13/5	0.81 (0.25–2.61)	0.727

In this table, the data of steroid resistance in the UC patients and the two polymorphisms are summarized. A significantly greater number of patients with the *NQO1* T/T genotype showed steroid resistance than the other genotypes ($p = 0.002$).

The *SOD2* gene is located on 6q25 (Church *et al.*, 1992). The *SOD2* Ala-9Val polymorphism has a structural mutation of a T-to-C substitution in the coding sequence that changes the amino acid codon at the −9 position in the signal peptide from valine to alanine (Shimoda-Matsubayashi *et al.*, 1996). The C allele may confer an advantage to the SOD2 protein, rendering C/C genotype and C/T genotype than the T/T genotype (Sutton *et al.*, 2003). The Ala-9Val polymorphism has been associated with various diseases, such as Parkinson's disease (Shimoda-Matsubayashi *et al.*, 1996), nonfamilial idiopathic cardiomyopathy (Hiroi *et al.*, 1999), breast cancer (Ambroson *et al.*, 1999), and colorectal cancer (Stoehlmacher *et al.*, 2002).

This study provided two interesting findings of the *NQO1* polymorphism associated with UC. First, a significantly greater number of patients with the *NQO1* T/T genotype showed steroid resistance than the other genotypes. Second, more patients with the *NQO1* T/T genotype contracted severe colitis than the other genotypes. According to a previous report, the T/T genotype for *NQO1* C609T polymorphism has a null phenotype. NQO1 plays a role as a superoxide scavenger. Because of its role, NQO1 protects against superoxide-induced toxicity. Kruidenier *et al.* (2003) reported that intestinal inflammation was accompanied by excessive production of reactive metabolites. In addition, nitric oxide synthase and xanthine oxidase were both associated with oxidative stress in IBD. No studies have yet shown that NQO1 directly influences oxidative stress in IBD. However, patients with the *NQO1* T/T genotype may not prevent oxidative stress in the intestinal mucosa because the T/T genotype suppresses the activity of this enzyme. The suppression of NQO1 may influence the severity of UC.

The precise mechanism of steroid resistance in UC remains unclear. About 20–30% of the patients with severe acute UC make a poor response to corticosteroids (Hyde and Jewell, 1997). Involvement of genetic polymorphisms has been previously reported. Farrell and Kelleher (2003) reviewed glucocorticoid resistance in IBD. This review focused on the molecular mechanism of glucocorticoid resistance for the multidrug resistance gene (*MDR1*). The *MDR1* gene codes for a drug efflux pump, P-glycoprotein (Hoffmeyer *et al.*, 2000). MDR1 expression was elevated in UC and CD patients who required bowel resection for failed medical therapy (Farrell *et al.*, 2000). This suggests that IBD patients who failed to respond to medical therapy might escape effective immunosuppression by steroids and other immunosuppressive agents, because these drugs were MDR substrates and were pumped out of the target cells due to P-glycoprotein–mediated efflux. The association between *MDR1* polymorphism and cyclospoline A failure was investigated in patients with steroid resistant UC (Daniel *et al.*, 2007). The TT genotype in exon 21 of *MDR1* was associated with a higher risk of cyclospoline A failure in these patients.

Single-nucleotide polymorphisms of Solute Carrier Family (*SLC*) *22A4/5* have received greater clinical attention because they can modulate their transporter functions, causing individual variations in drug responsiveness (Newman *et al.*, 2005). In a Japanese study, the association of *SLC22A4/5* with steroid responsiveness of IBD was investigated (Nakahara *et al.*, 2008). The CG haplotype, comprising the C allele of the −446C > T and −368T > G in *SLC22A5* appeared to be a predictor of steroid resistance in Japanese patients with CD.

The previous report proposed that the criteria to predict patients with severe UC would respond poorly to intensive medical treatment and require colectomy (Travis *et al.*, 1996). According to the criteria, patients with frequent stools (>8/day), or raised C-reactive protein (CRP) levels (>450 mg/L) after 3 days of intensive treatment, need to be identified, as most will require colectomy on that admission. The criteria suggested that patients with severe UC applied to the criteria would respond poorly to intravenous corticosteroid therapy and require colectomy. Severe colitis of UC may induce steroid resistance (Esteve *et al.*, 2008). However, severe colitis does not necessarily resulted in steroid resistance; it is thought that severe colitis is assumption of steroid resistance.

Several factors cause steroid resistance, including oxidative stress. It has been reported that oxidative stress affected steroid resistance because of reduced Histone deacetylase 2 (HDAC-2) activity (Marwick *et al.*, 2007). Chromatin is subjected to a variety of posttranslational modifications known as the histone code that ultimately affect gene transcription. This modification such as acetylation and deacetylation are programmed by two families of enzymes referred to as histone acetyltransferases and HDACs. HDAC-2 plays a pivotal role in corticoid action, and recruits corticosteroid through the glucocorticoid receptor. Under condition of oxidative stress, HDAC-2 is inactivated and cannot be recruited into the corepressor by glucocorticoid receptor. This mechanism results in steroid resistance. Patients with *NQO1* T/T genotype have insufficient prevention of oxidative stress. The insufficient prevention of oxidative stress causes steroid resistance in patients with *NQO1* T/T genotype.

In the patients with an age of onset at age 20 years or younger, more had the *SOD2* T/T genotype than the other genotypes, suggesting that the T/T genotype might be associated with the age of onset of UC. As for the significance of the relatively early disease onset, the *SOD2* gene might influence the onset of disease directly or by acting upon another gene or factor. However, Taufer *et al.* (2005) showed that the *SOD2* polymorphism was associated with DNA damage in association with oxidative stress. These authors assumed that SOD2 supported the free radical theory of aging. Another author suggested that the T allele resulted in less effective targeting of SOD2 (Shimoda-Matsubayashi *et al.*, 1996). Our results may indicate that this genotype is associated with insufficient prevention of oxidative stress, and the resulting increase in oxidative stress may cause the development of colitis at a younger age.

In conclusion, the *NQO1* C609T polymorphism may influence the severity of UC and steroid resistance in UC patients, while the *SOD2* Ala-9Val polymorphism may influence the age at onset of UC. Further studies are needed to investigate the effect of *NQO1* and *SOD2* polymorphisms on UC.

Disclosure Statement

No competing financial interests exist.

References

Akyol, O., Canatan, H., Yilmaz, H.R., Yuce, H., Ozyurt, H., Sogut, S., Gulec, M., and Elyas, H. (2004). PCR/RFLP-based cost-effective identification of SOD2 signal (leader) sequence

polymorphism(Ala-9Val) using *Ngo*M IV: a detailed methodological approach. Clin Chim Acta **245,** 151–159.

Ambrosone, C.B., Freudebeim, J.L., Thompson, P.A., Bowman, E., Vena, J.E., Marshall, J.R., Graham, S., Laughlin, R., Nemoto, T., and Shields, P.G. (1999). Manganese superoxide dismutase (MnSOD) genetic polymorphisms, dietary antioxidants, and risk of breast cancer. Cancer Res **59,** 602–606.

Church, S.L., Grant, J.W., Meese, E.U., and Trent, J.M. (1992). Sublocalization of the gene encoding manganese superoxide dismutase (MnSOD/SOD2) to 6q25 by fluorescence *in situ* hybridization and somatic cell hybrid mapping. Genomics **14,** 823–825.

Crapo, J.D., Oury, T., Rabouille, C., Slot, J.W., and Chang, L.Y. (1992). Copper, zinc superoxide dismutase is primarily a cytosolic protein in human cells. Proc Natl Acad Sci USA **89,** 10405–10409.

Daniel, F., Loriot, M.A., Seksik, P., Cosnes, J., Gornet, J.M., Lémann, M., Fein, F., Vernier-Massouille, G., De Vos, M., Boureille, A., Treton, X., Flouríe, B., Roblin, X., Louis, E., Zerbib, F., Beaune, P., and Marteau, P. (2007). Multidrug resistance gene-1 polymorphisms and resistance to cyclosporine A in patients with steroid resistant ulcerative colitis. Inflamm Bowel Dis **13,** 19–23.

Esteve, M., and Gisbert, J.P. (2008). Severe ulcerative colitis: at what point should we define resistance to steroids? World J Gastroenterol **14,** 5504–5507.

Farrell, R.J., and Kelleher, D. (2003). Mechanisms of steroid action and resistance in inflammation. Glucocorticoid resistance in inflammatory bowel disease. J Endocrinol **178,** 339–346.

Farrell, R.J., Murphy, A., Long, A., Donnelly, S., Cherikuri, A., O'Toole, D., Mahmud, N., Keeling, P.W., Weir, D.G., and Kelleher, D. (2000). High multidrug resistance (P-glycoprotein 170) expression in inflammatory bowel disease patients who fail medical therapy. Gastroenterology **118,** 279–288.

Guidot, D.M., McCord, J.M., Wright, R.M., and Repine, J.E. (1993). Absence of electron transport (Rho 0 state) restores growth of a manganese-superoxide dismutase-deficient *Saccharomyces cerevisiae* in hyperoxia: evidence for electron transport as a major source of superoxide generation *in vivo*. J Biol Chem **2678,** 26699–26703.

Hiroi, S., Harada, H., Nishi, H., Sato, M., Nagai, R., and Kimura, A. (1999). Polymorphisms in the SOD2 and HLA-DRB1 genes are associated with nonfamilial idiopathic dilated cardiomyopathy in Japanese. Biochem Biophys Res Commun **261,** 332–339.

Hoffmeyer, S., Burk, O., von Richter, O., Arnold, H.P., Brockmöller, J., Johne, A., Cascorbi, I., Gerloff, T., Roots, I., Eichelbaum, M., and Brinkmann, U. (2000). Functional polymorphisms of the human multidrug-resistance gene: multiple sequence variations and correlation of one allele with P-glycoprotein expression and activity *in vivo*. Proc Natl Acad Sci USA **97,** 3473–3478.

Hyde, G.M., and Jewell, D.P. (1997). The management of severe ulcerative colitis. Aliment Pharmacol Ther **11,** 419–424.

Jaiswal, A.K. (1991). Human NAD(P)H:quinone oxidoreductase (NQO1) gene structure and induction by dioxin. Biochemistry **30,** 10647–10653.

Koutroubakis, I.E., Malliaraki, N., Dimoulios, P.D., Karmiris, K., Castanas, E., and Kouroumalis, E.A. (2004). Decreased total and corrected antioxidant capacity in patients with inflammatory bowel disease. Dig Dis Sci **49,** 1433–1437.

Koutroubakis, I., Manousos, O.N., Meuwissen, S.G., and Pena, A.S. (1996). Environmental risk factors in inflammatory bowel disease. Hepatogastroentrerology **43,** 381–393.

Kruidenier, L., Kuiper, I., Lamers, C.B., and Verspaget, H.W. (2003). Intestinal oxidative damage in inflammatory bowel disease: semi-quantification, localization, and association with mucosal antioxidants. J Pathol **201,** 28–36.

Lafuente, M.J., Casterad, X., Trias, M., Ascaso, C., Molina, R., Ballesta, A., Zheng, S., Wiencke, J.K., and Lafuente, A. (2000). NAD(P)H:quinone oxidoreductase-dependent risk for colorectal cancer and its association with the presence of K-*ras* mutations in tumor. Carcinogenesis **21,** 1813–1819.

Larson, R.A., Wang, Y., Banerjee, M., Wiemels, J., Hartford, C., Le Beau, M.M., and Smith, M.T. (1999). Prevalence of the inactivating 609C → T polymorphism in the NAD(P)H:quinone oxidoreductase gene in patients with primary and therapy-related myeloid leukemia. Blood **94,** 803–807.

Marwick, J.A., Ito, K., Adcock, I.M., and Kirkham, P.A. (2007). Oxidative stress and steroid resistance in asthma and COPD: pharmacological manipulation of HDAC-2 as a therapeutic strategy. Expert Opin Ther Targets **11,** 745–755.

Nakahara, S., Arimura, Y., Saito, K., Goto, A., Motoya, S., Shinomura, Y., Miyamoto, A., and Imai, K. (2008). Association of SLC22A4/5 polymorphisms with steroid responsiveness of inflammatory bowel disease in inflammatory bowel disease in Japan. Dis Col Rec **51,** 598–603.

Naoe, T., Takeyama, K., Yokozawa, T., Kiyoi, H., Seto, M., Uike, N., Ino, T., Utsunomiya, A., Maruta, A., Jin-nai, I., Kamada, N., Kubota, Y., Nakamura, H., Shimazaki, C., Horiike, S., Kodera, Y., Saito, H., Ueda, R., Wiemels, J., and Ohno, R. (2000). Analysis of genetic polymorphism in *NQO1, GST-M1, GST-T1,* and *CYP3A4* in 469 Japanese patients with therapy-related leukemia/myelodysplastic syndrome and *de novo* acute myeloid leukemia. Clin Cancer Res **6,** 4091–4095.

Newman, B., Gu, X., Wintle, R., Cescon, D., Yazdanpanah, M., Liu, X., Peltekova, V., van Oene, M., Amos, C.I., and Siminovitch, K.A. (2005). A risk haplotype in the Solute Carrier Family 22A4/22A5 gene cluster influences phenotypic expression of Crohn's disease. Gastroenterology **128,** 260–269.

Olson, S.H., Carlson, M.D., Ostrer, H., Harlap, S., Stone, A., Winters, M., and Ambrosone, C.B. (2004). Genetic variants in *SOD2, MPO,* and *NQO1,* and risk of ovarian cancer. Gynecol Oncol **93,** 615–620.

Orchard, T.R., Satsangi, J., Van Heel, D., and Jewell, D.P. (2000). Genetics of inflammatory bowel disease: a reappraisal. Scand J Immunol **51,** 10–17.

Phillips, R.M., Basu, S., Brown, J.E., Flannigan, G.M., Loadman, P.M., Martin, S.W., Naylor, B., Puri, R., and Shah, T. (2004). Detection of (NAD(P)H:quinone oxidoreductase-1, EC1.6.99.2) 609C → T and 459C → T polymorphisms in formalin-fixed, paraffin-embedded human tumour tissue using PCR-RFLP. Int J Oncol **24,** 1005–1010.

Ross, D., Kepa, J.K., Winski, S.L., Beall, H.D., Anwar, A., and Siegel, D. (2000). NAD(P)H:quinone oxidoreductase 1 (NQO1): chemoprotection, bioactivation, gene regulation and genetic polymorphisms. Chem Biol Interact **129,** 77–97.

Shimoda-Matsubayashi, S., Matsumine, H., Kobayashi, T., Nakagawa-Hattori, Y., Shimizu, Y., and Mizuno, Y. (1996). Structural dimorphism in the mitochondrial targeting sequence in the human manganese superoxide dismutase gene. A predictive evidence for conformational change to influence mitochondrial transport and a study of allelic in Parkinson's disease. Biochem Biophys Res Commun **226,** 561–565.

Siegel, D., McGuinness, S.M., Winski, S.L., and Ross, D. (1999). Genotype-phenotype relationships in studies of a polymorphism in NAD(P)H:quinone oxidoreductase 1. Pharmacogenetics **9,** 113–121.

Silverberg, M.S., Cho, J.H., Rioux, J.D., McGovern, D.P., Wu, J., Annese, V., Achkar, J.P., Goyette, P., Scott, R., Xu, W.,

Barmada, M.M., Kiel, L., Daly, M.J., Abraham, C., Bayless, T.M., Bossa, F., Griffiths, A.M., Ippoliti, A.F., Lahaie, R.G., Latiano, A., Paré, P., Proctor, D.D., Regueiro, M.D., Steinhart, A.H., Targan, S.R., Schumm, L.P., Kistner, E.O., Lee, A.T., Gregersen, P.K., Rotter, J.I., Brant, S.R., Taylor, K.D., Roeder, K., and Duerr, R.H. (2009). Ulcerative colitis-risk loci on chromosomes 1p36 and 12q15 found by genome-wide association study. Nat Genet **41,** 216–220.

Stoehlmacher, J., Ingles, S.A., Park, D.J., Zhang, W., and Lenz, H.J. (2002). The -9Ala/-9Val polymorphism in the mitochondrial targeting sequence of the manganese superoxide dismutase gene (MnSOD) is associated with age among Hispanics with colorectal carcinoma. Oncol Rep **9,** 235–238.

Sutton, A., Khoury, H., Prip-Buus, C., Cepanec, C., Pessavre, D., and Deqoul, F. (2003). The Ala 16 Val genetic dimorphism modulates the import of human manganese super oxide dismutase in amyotrophic rat liver mitochondria. Pharmacogenetics **13,** 145–157.

Taufer, M., Peres, A., de Andrade, V.M., de Oliveira, G., Sá, G., do Canto, M.E.P., dos Santos, A.R., Bauer, M.E., and da Cruz, I.B.M. (2005). Is the Val16Ala manganese superoxide dismutase polymorphism with the aging process? J Gerontol **60,** 432–438.

Traver, R.D., Siegel, D., Beall, H.D., Phillips, R.M., Gibson, N.W., Franklin, W.A., and Ross, D. (1997). Characterization of a polymorphism in NAD(P)H:quinone oxidoreductase (DT-diaphorase). Br J Cancer **75,** 69–75.

Travis, S.P., Farrant, J.M., Ricketts, C., Nolan, D.J., Mortensen, N.M., Kettlewell, M.G., and Jewell, D.P. (1996). Predicting outcome in severe ulcerative colitis. Gut **38,** 905–910.

Truelove, S.C., Willoughby, C.P., Lee, E.G., and Ketlewell, M.G. (1978). Further experience in the treatment in the severe attacks of ulcerative colitis. Lancet **2,** 1086–1088.

Zelko, I.N., Mariani, T.J., and Folz, R.J. (2002). Superoxide dismutase multigene family: a comparison of the CuZn-SOD (SOD1), Mn-SOD (SOD2), and EC-SOD (SOD3) gene structures, evolution, and expression. Free Radic Biol Med **33,** 337–349.

Zhang, J.H., Li, Y., Wang, R., Geddert, H., Guo, W., Wen, D.G., Chen, Z.F., Wei, L.Z., Kuang, G., He, M., Zhang, L.W., Wu, M.L., and Wang, S.J. (2003). NQO1C609T polymorphism associated with esophageal cancer and gastric cardiac carcinoma in North China. World J Gastroenterol **9,** 1390–1393.

Address correspondence to:
Junji Yoshino, M.D.
Department of Internal Medicine
Second Teaching Hospital Fujita Health University
School of Medicine
3-6-10 Otobashi, Nakagawaku
Nagoya 454-8509
Japan

E-mail: jyoshino@fujita-hu.ac.jp

Received for publication February 25, 2009; received in revised form July 2, 2009; accepted July 2, 2009.

Original Article

Cytogenetic and Genome Research

Cytogenet Genome Res 2009;125:201–212
DOI: 10.1159/000230004

Accepted after revision: March 13, 2009
by M. Schmid

The Chromosomal Constitution of Postmitotic Neurons, Assessed by Neuronal Nuclear Transfer into Oocytes and in ES Cell Lines Derived from Them

T. Osada[a–c] N. Kakazu[d] M. Watanabe[e] H. Yamane[d] T. Yagi[b, c]

[a]Department of Regenerative and Developmental Biology, Mitsubishi Kagaku Institute for Life Sciences (MITILS), Tokyo; [b]CREST Research Agency, JST, [c]KOKORO Biology Group, Department of Integrated Biology, Graduate School of Frontier Biosciences, Osaka University, Osaka; [d]Department of Environmental and Preventive Medicine, Shimane University School of Medicine, Izumo City; [e]Laboratory for Medical Engineering, Division of Materials Science and Chemical Engineering, Graduate School of Engineering, Yokohama National University, Yokohama, Japan

Key Words
Chromatin condensation · Chromosomes · Embryonic stem cells · Nuclear transfer · SKY

Abstract
Spectral karyotyping (SKY) was used to assess the chromosomal constitution of embryos generated by nuclear transfer (NT) of neuronal nuclei (N-NT) or cumulus cell nuclei (C-NT) into oocytes and of their embryonic stem cell derivatives (ntES cells). We detected chromosomal changes during the first mitotic cleavage and in the condensed chromatids of NT embryos. We also found clonal translocations in the ntES cells that were derived from NT embryos cloned from neuronal nuclei. The differentiation potentials of the ntES cells showing chromosomal rearrangements were partly restricted. Our findings indicate that balanced or unbalanced chromosomal translocations can occur in early NT embryogenesis, suggesting that a DNA repair system is activated during both NT embryogenesis and ntES cell establishment. We observed a higher incidence of chromosomal changes in N-NT than in C-NT embryos, which may reflect a higher frequency of double-stranded (ds) DNA breaks in the neuronal genome.

Although condensed chromosomes are not visible in postmitotic cells, technology allowing the visualization of whole chromosome sets provides important genetic information about DNA mutations associated with physiology and disease. A wealth of studies has indicated that chromosomes are susceptible to age-related DNA damage [Johnson et al., 1999; Albert et al., 2002] and cell death [Gossen et al., 1989]. DNA variation among individuals was recently discovered and put forward as a mechanism for genetic diversity [Redon et al., 2006]. Although DNA recombination in the neuronal genome, analogous to that occurring in the immune system, has been postulated to contribute to neuronal identity [Chun et al., 1991], no definitive evidence for this activity has been reported. Instead, recent analyses have reported chromosomal aneuploidy in neural subpopulations [Rehen et al., 2001] and the integration of retrotransposable elements in CNS cells [Muotri et al., 2005]. Although the biological significance of these discoveries remains unclear, they are fascinating phenomena with potentially significant implications for neuronal complexity [Mattick and Mehler, 2008]. To analyze the genetic codes of individual neurons, however, a genetic source, i.e. a large collection of cell lines cloned from the DNA of single neurons, is needed.

KARGER

Fax +41 61 306 12 34
E-Mail karger@karger.ch
www.karger.com

1424–8581/09/1253–0201$26.00/0

Accessible online at:
www.karger.com/cgr

Tomoharu Osada, DVM, PhD
Department of Regenerative and Developmental Biology
Mitsubishi Kagaku Institute of Life Sciences
11 Minamiooya, Machida-shi, Tokyo 194-8511 (Japan)
Tel. +81 42 724 6250, Fax +81 42 724 6314, E-Mail tomoosada@gmail.com

Table 1. SKY analysis of nuclear transferred ES cell lines

ES cell line	Donor nuclei	Strain	Sex	Karyotypes		
				analyzed	normal (%)	clonal translocation [n, %]
Cam-1	pyramidal neurons	C57Bl/6 × [(C57Bl/6 × DBA/2) × DBA/2]N2	XY	4	2 (50)	
Cam-2	pyramidal neurons	C57Bl/6 × [(C57Bl/6 × DBA/2) × DBA/2]N2	XY	17	10 (59)	T(11;13) [4, 23]
Nex-1	pyramidal neurons	C57Bl/6 × [(C57Bl/6 × DBA/2) × DBA/2]N3	XY	18	12 (67)	
Nex-2	pyramidal neurons	C57Bl/6 × [(C57Bl/6 × DBA/2) × DBA/2]N3	XY	12	0 (0)	T(1;6); der(4)T(4;6) [12, 100]
Gad67-1	GABAnergic neurons	DBA/2 × C57Bl/6	XY	19	12 (63)	
Gad67-2	GABAnergic neurons	DBA/2 × C57Bl/6	XX	5	1 (20)	
Cum-1	cumulus cells	DBA/2 × C57Bl/6	XX	10	2 (20)	
TT2		CBA × C57Bl/6	XY	10	6 (60)	

Several methodologies have been developed to analyze single cell-derived DNA. First, a transgenic mouse mutation detection system was developed to assess directly mutations in the genome of postmitotic cells in vivo [Gossen et al., 1989]. This approach enables the detection of radiation-induced DNA damage in somatic cells, but it may not be able to disclose site-specific mutations in the genome. An alternative approach was developed to visualize the entire chromosomal constitution of a single postmitotic cell by means of nuclear transfer (NT) [Osada et al., 2002]. In the original experiment, mammalian oocytes were used as a biological container in which to examine the chromosome constitution of sperm [Rudak et al., 1978; Lee et al., 1996]. We previously applied NT to the analysis of neuronal genomes [Osada et al., 2002], and our findings suggested that chromosomal changes could occur in embryos generated by NT of neuronal nuclei (N-NT embryos) during the first mitotic cleavage. In the present study, we used spectral karyotyping (SKY) [Liyanage et al., 1996] to examine the karyotypes of N-NT embryos during condensed chromatid formation and the first mitotic cleavage, and of those cell lines derived from N-NT embryos.

Materials and Methods

Mice and ES Cells

Recipient oocytes were collected from B6D2F1 hybrid mice. Donor neurons were collected from B6 transgenic mice that expressed green fluorescence protein (GFP) specifically in pyramidal neurons resulting from the use of a genetic marking system [Osada et al., 2005]. Six ntES cell lines derived from the nuclei of neurons (Cam-1, -2, Nex-1, -2, and Gad67-1, -2) and 1 ntES cell line from cumulus cells (Cum-1) were examined in this study (table 1). These cells were cultivated with feeder cells and TT2 ES cells were used as control. The TT2 ES cells were derived from blastocysts of an F1 hybrid mouse strain (CBA × C57BL/6) and showed pluripotency in chimeras, including the ability to form germ lines [Yagi et al., 1993].

Nuclear Transfer and Mitotic Spread Preparation

Nuclear transfer experiments were carried out as described previously [Osada et al., 2005]. To obtain the condensed chromatids, cells were collected and fixed 2–3 h after injection of the donor nuclei into enucleated oocytes. To obtain metaphase chromosomes, NT embryos during the first mitotic cleavage, and ES cells derived from NT embryos were collected (fig. 1). Metaphase spreads from the N-NT embryos were prepared with a standard method [Mikamo et al., 1983]. The zona pellucida of the N-NT oocytes was digested with actinase (Kaken Pharmaceutical Co., Ltd., Tokyo, Japan). After washing with PBS, the cells were transferred to a hypotonic solution (0.075 mM citric acid:10% FBS, 1:1). The expanded cells were fixed with modified Carnoy's fixative and promptly spread on glass slides. To obtain mitotic spreads from the first cleavage, the N-NT embryos were incubated for 6–7 h after activation in CZB medium containing 6 nM vinblastine sulfate.

ES Cell Culture

ES cells were cultured and maintained under standard conditions [Hogan et al., 1994]. The culture medium for cloned ES cells was composed of 17.5% KnockOut Serum Supplement (KSR), 100 μM non-essential amino acids, 1 mM pyruvate (all from Invitrogen, Carlsbad, CA), 0.1 mM β-mercaptoethanol (Wako, Osaka, Japan), and 1,000 IU/ml leukemia inhibitory factor (LIF) in KnockOut D-MEM (Invitrogen). The TT2 ES cells were cultured in the same medium with the same components, except that 20% fetal bovine serum (Invitrogen) was used instead of KSR. The feeder cells were prepared from embryonic fibroblasts obtained from a BALB/c inbred mouse strain on embryonic day (E) 13.5 and treated with 10 μg/ml mitomycin C (Sigma, St. Louis, MO) for at least 2 h. The cells were passaged approximately every 4 days.

Metaphase Spread Preparation

After 6–9 passages ES cells at metaphase were used for the preparation of metaphase spreads with a standard method [Kakazu et al., 1999]. The ES cells were treated with colcemid (Invitrogen) at 0.1 μg/ml final concentration for 1 h. Mitotically arrested cells were subjected to hypotonic treatment (0.075 M KCl)

or 30 min, fixed by changing the solution with Carnoy's fixative methanol:acetic acid = 3:1, v/v) 3 times, after which the solution containing the cells was spread on a glass slide.

Spectral Karyotyping (SKY)

The metaphase cells were subjected to SKY analysis. The mouse SKY paint probe mixture (Applied Spectral Imaging, Migdal Ha'Emek, Israel), which contains combinatorially labeled painting probes specific for each of the 21 mouse chromosomes, was used for hybridization. Hybridization and detection were carried out as described elsewhere [Kakazu et al., 1999]. The chromosomes were counterstained with 4′,6-diamidino-2-phenylindole dihydrochloride (DAPI).

Fluorescence in situ Hybridization (FISH) Analyses

To narrow down the 6q breakpoint region of T(1;6) in the Nex-2 NT-ES cells, we performed sequential FISH analyses using 11 bacterial artificial chromosome (BAC) probes located on chromosome 6q. The BAC clones (RP23 series) on chromosome 6q were selected according to the University of California Santa Cruz (UCSC) Genome Browser (http://genome.ucsc.edu), and were directly labeled with SpectrumOrange-dUTP (Abbott Molecular/Vysis, Des Plaines, IL). To identify normal and translocated chromosomes 1, RP23-374B10 (located at chromosome 1qA1) labeled with SpectrumOrange-dUTP (Abbott Molecular/Vysis) was used together with the chromosome 6q probes. Hybridization, washing, and detection were performed as described previously [Kakazu et al., 1999]. Chromosomes were counterstained with DAPI. FISH images were captured and analyzed with the PowerGene system (Applied Imaging).

Differentiation of ES Cells in vitro and in vivo

The differentiation of ES cells in vitro was induced by retinoic acid, as described previously [Bain et al., 1995]. Briefly, after 2 days in vitro, the ES cells were trypsinized and dispersed into the culture medium without LIF or β-mercaptoethanol and with trans-retinoic acid (1 μM, Sigma). On the 4th day after addition of the retinoic acid, the embryoid bodies (EBs) that had developed were transferred onto a laminin/poly-L-lysine (1:1)-coated Petri dish containing the same medium, but without retinoic acid. The cells were collected and analyzed after 7 days of culture.

For the subcutaneous injection of ES cells into nude mice, ES cells were grown under normal conditions for 3 days. The cells were then gently trypsinized, and 1–2 × 10^6 cells were injected subcutaneously into each flank of 6–8-week-old female BALB/c *nu/nu* mice (Oriental Yeast, Tokyo, Japan). 3–5 weeks after injection, the mice were euthanized, decapitated and the tumors collected. The obtained tumors were weighed and fixed with either 10% neutralized formalin solution or Bouin's solution.

Immunofluorescence

Indirect immunofluorescence analyses of the differentiated cells were performed on the 8th day of culture on a laminin/lysine-coated Petri dish, and of undifferentiated cells on the 4th day of culture with feeder cells. The cells were fixed with 4% paraformaldehyde for 30 min at room temperature (RT) and then permeabilized with PBS containing 0.05% Tween-20 and 0.5% Triton X-100 for 20 min at RT. After blocking with PBS containing 0.05% Tween-20 and 10% normal goat serum for 1 h, the cells were incubated with antibodies to NeuN (1:100, Chemicon International, Temecula, CA), GAD67 (1:400, Chemicon), or Desmin (1:50, Sigma) overnight. After incubation with the secondary antibodies, which were conjugated with Alexafluor 594 (Molecular Probes, Eugene, OR), the cells were stained with DAPI and observed under a fluorescence microscope (IX51; Olympus, Tokyo, Japan).

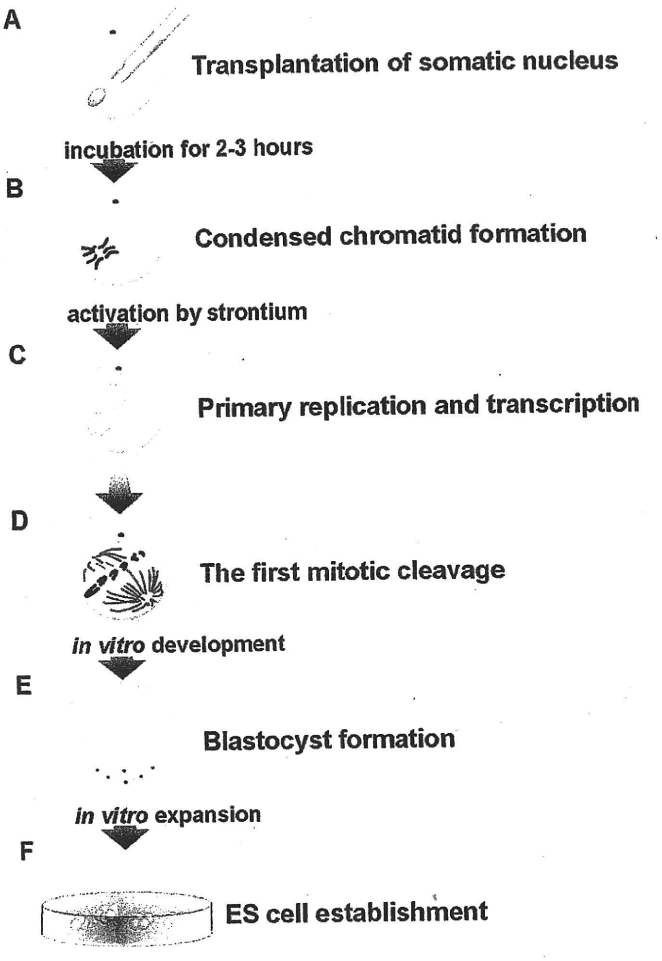

Fig. 1. Diagram of the developmental stages at which condensed chromatids/chromosomes were examined. After its injection into the ooplasm (**A**), donor nuclear DNA condenses within 2–3 h (**B**). Because the injected DNA is not replicated during this period, the DNA forms condensed chromatids. After activation stimulation by strontium, the reconstructed NT embryos form pseudo-pronuclei where the primary replication and transcription progress (**C**). Mitotic spreads are prepared during the first embryonic cleavage (**D**). Some of the N-NT embryos develop into blastocysts (**E**). The inner cell mass is expanded in vitro, and the N-ntES cells are established after sequential passages (**F**). Mitotic spreads are prepared from the N-ntES cells after 6–9 passages.

Table 2. SKY analysis of chromosomes from the N-NT and C-NT embryos during the first cleavage

Donor cells	No. of karyotypes analyzed	No. of informative karyotypes	No. (%) of normal karyotypes	Abnormal karyotypes	
				aneuploidy (indicated by number of chromosomes)	translocation (indicated by karyotypes)
Cortical neurons (N-NT)	87	25	20 (80)	36, 38, 39	T(1;12); T(6;13)
Cumulus cells (C-NT)	35	10	9 (90)	39	

Table 3. G-banding analysis of enucleated oocytes 3 h after injection of cumulus cell nuclei and adult cortical neuronal nuclei

Donor cells	No. of PCC analyzed	No. (%) of normal PCC	No. (%) of abnormal PCCs							
			with chromosome fragment			without chromosome fragment		with undercondensed chromatids		
			40 chr. (SA)	<40 chr.	>40 chr. (SA + NA)	<40 chr. (NA)	>40 chr. (NA)	<40 chr.	40 chr.	>40 chr.
Cortical neurons	92	47 (51)[a]	9 (10)	14 (15)[b]	1 (1)	17 (18)	2 (2)	1 (1)	1 (1)	0 (0)
Cumulus cells	48	39 (81)[a]	6 (13)	0 (0)[b]	0 (0)	3 (6)	0 (0)	0 (0)	0 (0)	0 (0)

Abbreviations: PCC, premature chromosome condensation; SA, structural chromosome aberrations; NA, numerical chromosome aberrations (aneuploidy).

[a] $p < 0.005$; [b] $p < 0.01$.

Reverse Transcription Polymerase Chain Reaction (RT-PCR)

Total RNA was isolated from each ES cell line (4-day cultures) and their derivatives (8-day culture on a laminin/lysine-coated Petri dish) by Trizol Reagent (Invitrogen). The cDNA was synthesized with the aid of Superscript III (Invitrogen) using oligo$(dT)_n$ primers, according to the manufacturer's instructions. The synthesized DNA was amplified as follows: 1 min at 94°C, then 30 cycles of 30 s at 94°C, 30 s at 55°C, and 1 min at 72°C, followed by a 10-min extension at 72°C. Hypoxanthine guanine phosphoribosyl transferase 1 *(Hprt1)* was used as a positive control. The primer sequences used for this assay and the length of the amplified DNA fragments were as follows:

POU domain, class 5, transcription factor 1 *(Pou5f1*, synonym *Oct-3/4)*: F 5′-CTTCTGCAGGGCTTTCATGT-3′, R 5′-TGTGGACCTCAGGTTGGACT-3′, 72 bp. Alpha-fetoprotein *(Afp)*: F 5′-ACCAGACCTTAGGAGACTAC-3′, R 5′-CACTCTTCCTTCTGGAGATG-3′, 596 bp. Transthyretin *(Ttr)*: F 5′-AAATCGTACTGGAAGACACT-3′, R 5′-ACTCTGCTTTCTGACCTATC-3′, 510 bp. Myosin heavy chain cardiac muscle 6 *(Myh6)*: F 5′AGATGCACTGGAGAAGTCTG-3′, R 5′-CAGCCATCTCCTCTGTTAGG-3′, 371 bp. Glial fibrillary acid protein *(Gfap)*: F 5′-CAAACACGAAGCTAACGACT-3′, R 5′-CCACAGTCTTTACCACGATG-3′, 407 bp. Glutamate receptor; ionotropic, AMPA1 (alpha1) *(Gria1)*: F 5′-CCAATTTGAAGGCAATGACC-3′, R 5′-TCTTCTCAAACACAGCGATT-3′, 770 bp. Gamma-aminobutyric acid (GABA) A receptor, subunit beta 1 *(Gabrb1)*: F 5′-GGGGCTTCTCTCTTTTCCCGTGA-3′, R 5′-GGTGTCTGGTACCCAGAGTTGGT-3′, 334 bp. *Hprt1*: F 5′-TTGTTGGATATGCCCTTGAC-3′, R 5′-GGAAATCGAGAGCTTCAGAC-3′, 506 bp.

Aliquots (5 μl) of the PCR mixture were analyzed by electrophoresis on 1–1.5% agarose gels stained with 0.5 μg/ml ethidium bromide.

Results

SKY Analyses during the First Mitotic Cleavage of N-NT Embryos

We first wanted to examine if the chromosomal changes in the N-ntES cells were detectable in early development. To this end, metaphase spreads prepared during the first mitotic cleavage of the N-NT and C-NT embryos were subjected to SKY analysis. Aneuploidy was detected in both the N-NT and C-NT embryos. In contrast to our previous findings [Osada et al., 2002] the frequency of aneuploidy in the N-NT and C-NT embryos was similar (table 2). On the other hand, a balanced translocation between chromosomes 6 and 13, T(6;13) (data not shown), and a balanced translocation between chromosomes 1 and 12, T(1;12) (fig. 2), were observed in the N-NT embryos

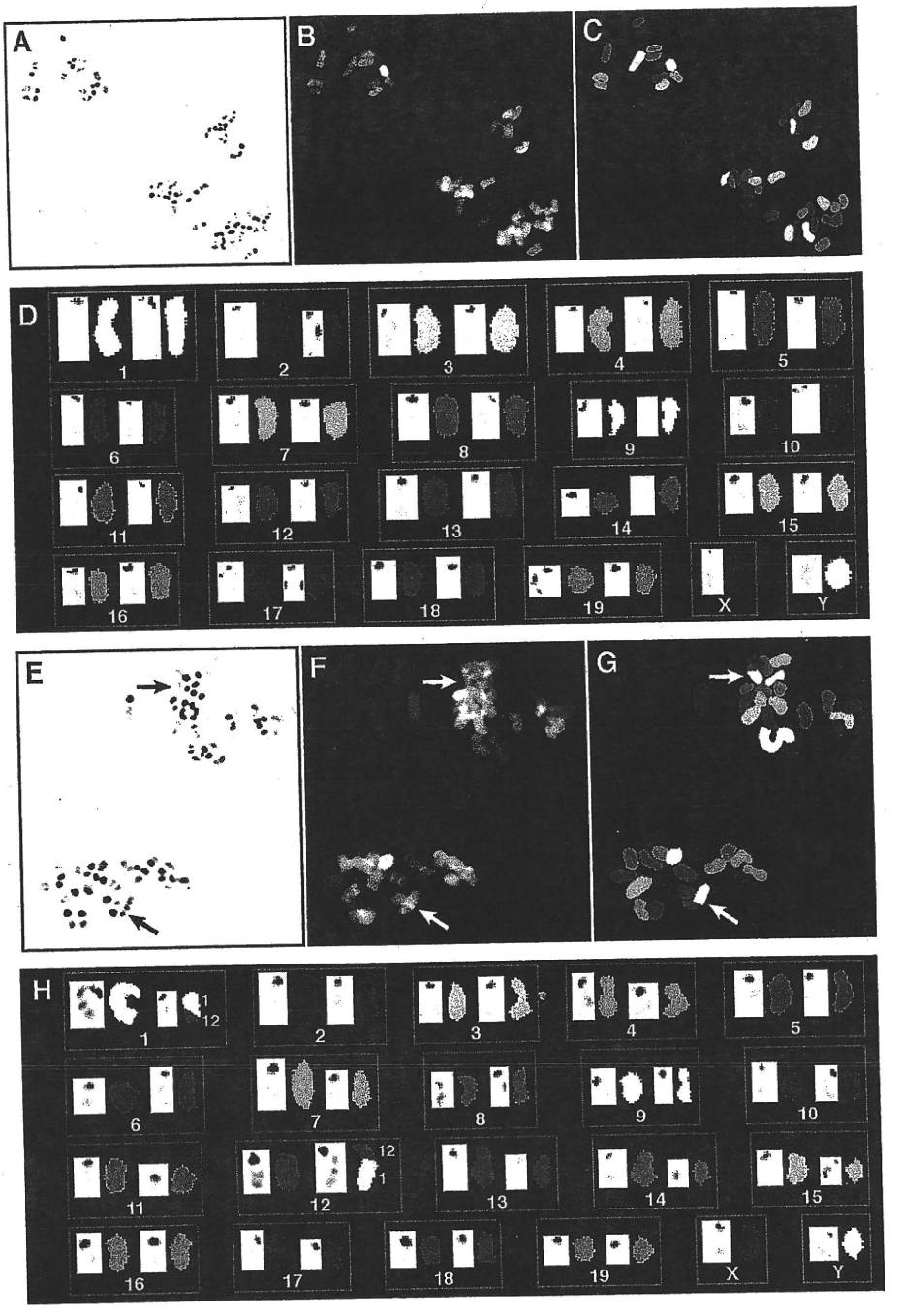

Fig. 2. SKY analysis of eggs at the first mitosis after injection of nuclei from adult cerebral neurons. **A–D** Metaphase spread with a normal chromosome set. **E–H** Metaphase spread with a balanced translocation between chromosomes 1 and 12, T(1;12). Images from left to right show inverted DAPI (**A**, **E**), spectral color (**B**, **F**), and classification color images (**C**, **G**). **D**, **H** Karyotype tables produced by combining SKY and DAPI banding. For each chromosome in the tables, G-band-like images are shown on the left and classified color images on the right. The numbers next to the classification color images in **H** indicate the origin of the chromosomal material. **E–G** Arrows indicate chromosomes with T(1;12).

(table 2), whereas no chromosomal changes were detected in the mitotic spreads prepared from the C-NT embryos.

SKY Analyses of the Condensed Chromatids after Injection of a Neuronal or Cumulus Cell Nucleus

Chromosomes from somatic cell nuclei form chromatid-like structures in the ooplasm upon their transfer into enucleated oocytes via M-phase promoting factor (MPF) [Ziegler and Masui, 1973]. Since this appears to be a biological window for assessment, prior to SKY analysis of the karyotype of donor nuclei by NT with a minimal influence from oocyte factors, aneuploidy of the chromatids was assessed by means of Giemsa staining (table 3). Fragmentation was observed in the chro-

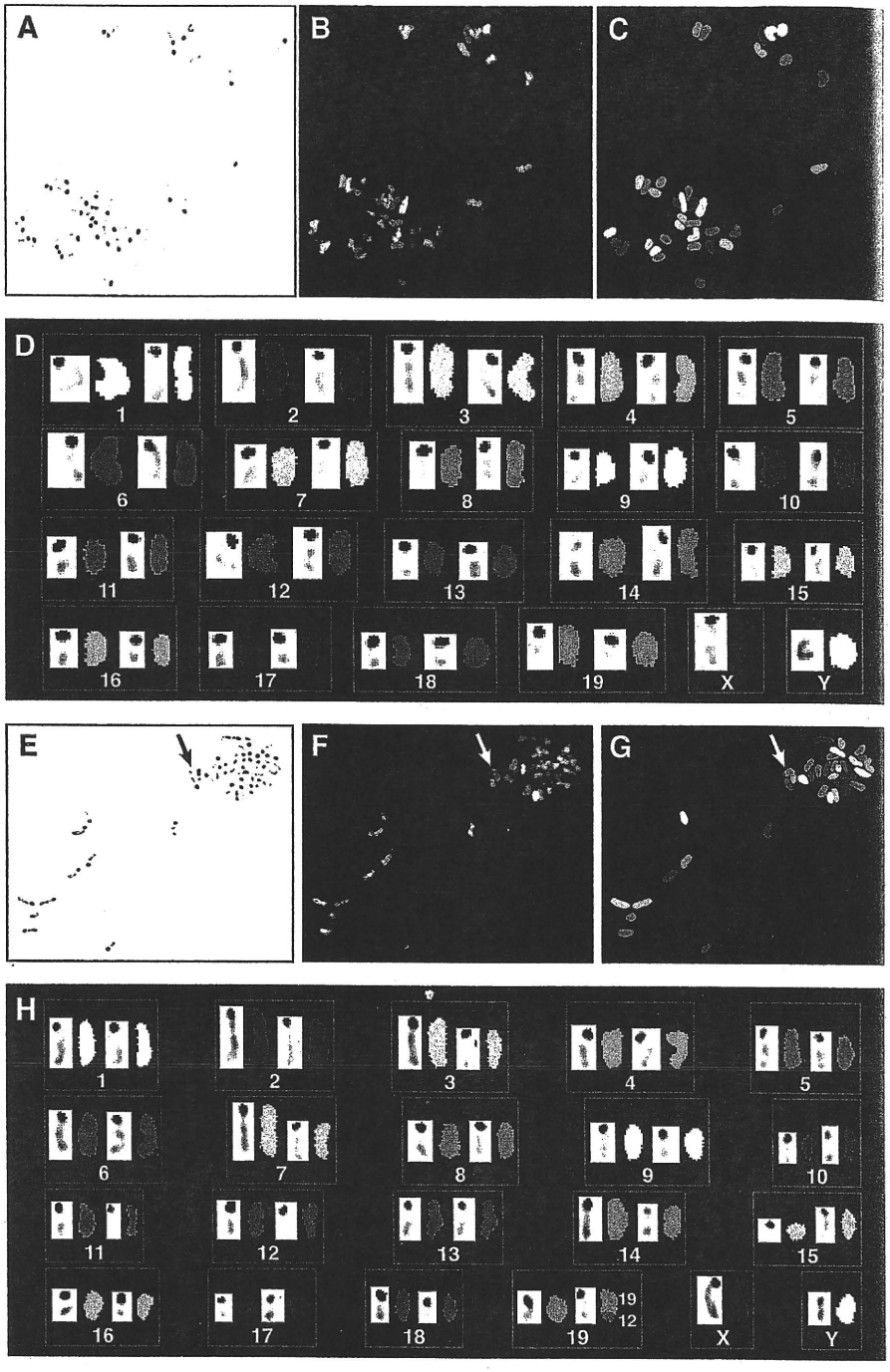

Fig. 3. SKY analysis of the condensed chromatids of oocytes injected with the nuclei of adult cerebral neurons. **A–D** Metaphase spread of a nucleus-injected oocyte without chromosomal aberrations. **E–H** Metaphase spread with an abnormal set of condensed chromatids of an oocyte injected with a neuronal nucleus. Note the presence of an unbalanced translocation, der(19)T(12;19) (**H**), indicated by arrows in **E–G**. For arrangement of images see legend of figure 2.

matid preparations from oocytes bearing neuronal or cumulus cell nuclei. A loss of chromosomes was observed in the neuron-derived condensed chromatids as reported previously [Osada et al., 2002]. Undercondensed chromatin was also detected, but with a lower frequency than in our previous study [Osada et al., 2002]. SKY painting of the chromatid preparations (fig. 3) showed the presence of unbalanced chromosomal changes in 3 of the 23 metaphase cells analyzed among the oocytes bearing a neuronal nucleus, including 2 showing an unbalanced translocation between chromosomes 12 and 19 (table 4, fig. 3E–H). This translocation

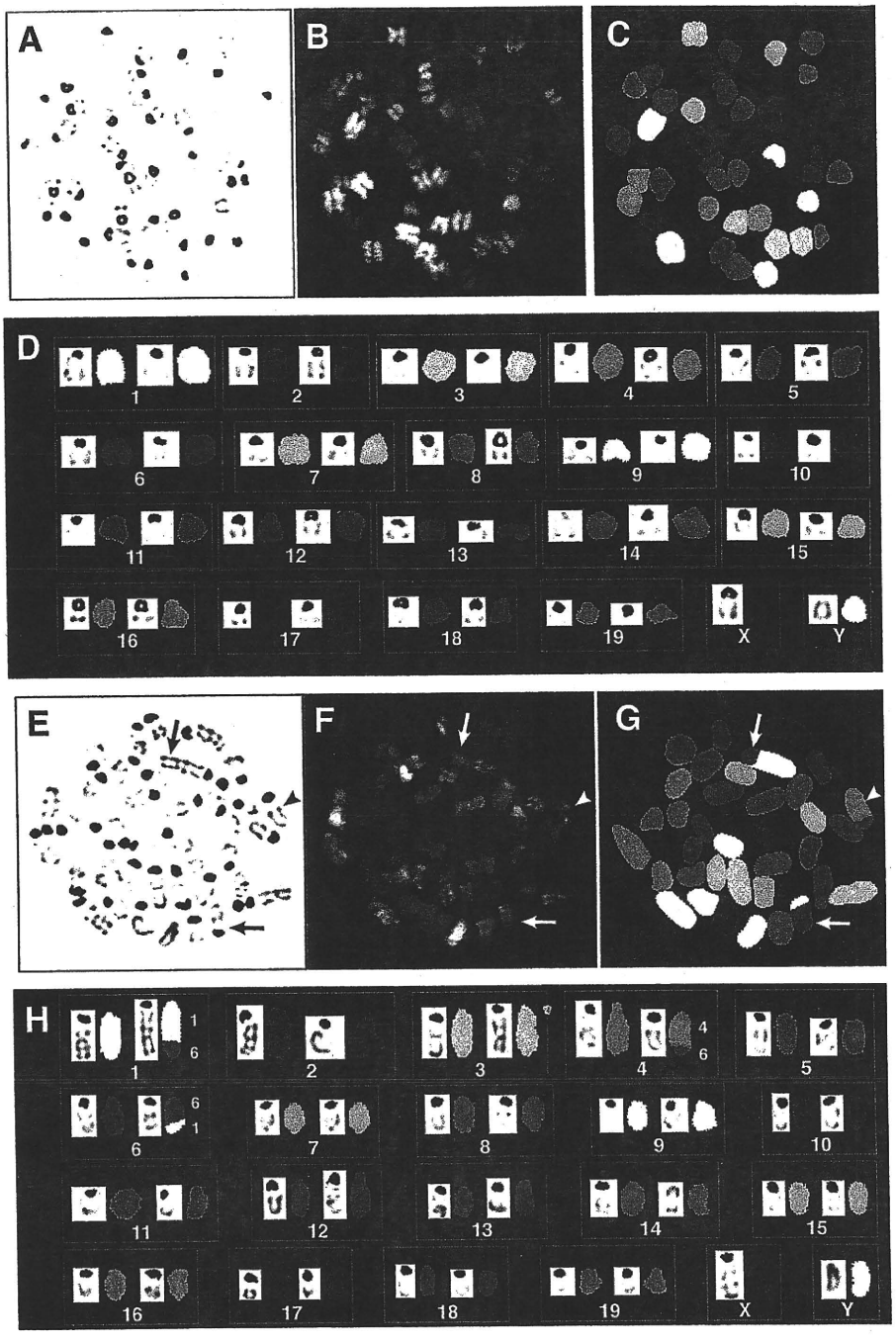

Fig. 4. SKY analysis of N-ntES cell lines Cam-2 (**A–D**) and Nex-2 (**E–H**). Arrows indicate chromosomes with a balanced translocation between chromosomes 1 and 6, T(1;6), arrowheads indicate the derivative chromosome 4 with an unbalanced translocation between chromosomes 4 and 6, der(4)T(4;6) (**E–G**). For arrangement of images see legend of figure 2.

Table 4. SKY analysis of premature chromatin condensations in the enucleate oocytes 3 h after injection

Donor cells	No. of PCC analyzed	No. of informative PCC	No. (%) of normal PCC	Abnormal PCC		
				fragments (indicated by number of karyotypes)	aneuploidy [n] (indicated by number of chromosomes)	translocation [n] (indicated by karyotypes)
Cortical neurons	93	23	17 (74)	2	36 [2]	der(19)T(12;19) [2]
Cumulus cells	47	15	13 (87)	0	39, 36	

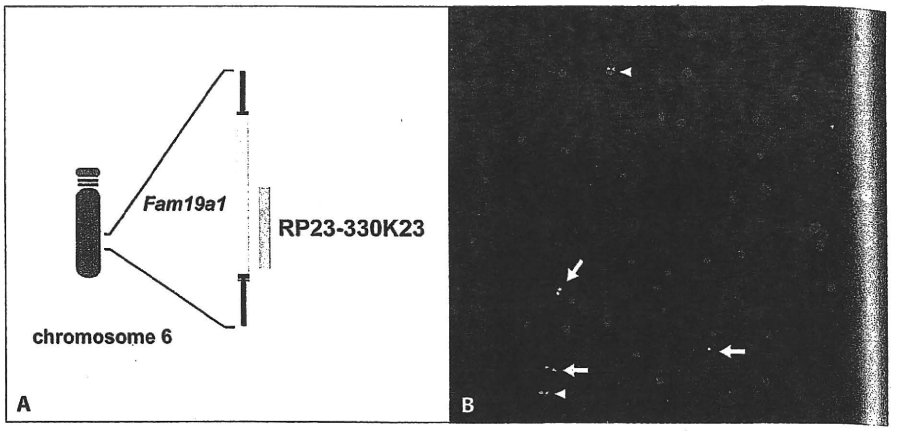

Fig. 5. A Schematic representation of the *Fam19a1* genomic region on mouse chromosome 6 and the position of the BAC probe RP23-330K23 used in this FISH analysis. **B** FISH analysis using the green-labeled RP23-330K23 probe (6qD3; arrows) together with the red-labeled RP23-374B10 probe (1qA1; arrowheads). Split green signals are detected on both the derivative chromosomes 1 and 6 in addition to the green signal on normal chromosome 6 in metaphases from Nex-2 NT-ES cells, indicating that RP23-330K23 spans the 6q breakpoint of T(1;6). The RP23-374B10 probe (red signal) was used for identification of normal and translocated chromosomes 1.

resulted in partial trisomy of the distal end of chromosome 12.

SKY Karyotyping of the ntES Cells Derived from N-NT Embryo (N-ntES) cells

We also used ntES cells derived from N-NT embryos at metaphase for SKY karyotyping [Osada et al., 2005]. SKY analysis of 8 ntES cell lines detected 2 clonal chromosomal abnormalities in Cam-2 and Nex-2 ntES cell lines (table 1). SKY analysis of the Cam-2 ES cells identified a normal karyotype in the majority of metaphases (59%) (fig. 4A–D) and 1 clonal balanced translocation, T(11;13) (data not shown), in another population of metaphase cells. SKY analysis of Nex-2 cells revealed a balanced translocation, T(1;6), and a derivative chromosome 4, der(4)T(4;6), from an unbalanced translocation between chromosomes 4 and 6 in all metaphase cells analyzed (fig. 4E–H). In contrast, no obvious clonal chromosomal abnormalities were detected in the control TT2 ES cells. The karyotypes of the Nex-1 line were normal in the major metaphase population (67%). Another population showed aneuploidy, with chromosomal numbers ranging from 46 to 76. Besides the structural and numerical chromosomal changes, the SKY analyses also detected metaphases with separated sister chromatids, also known as premature chromatid separation (PCS) [Hogan et al., 1994] in 5 ES cell lines (online supplementary fig. S1; for online supplementary material, see www.karger.com/doi/000230004).

FISH Analyses

The 6q breakpoint region of T(1;6) in the Nex-2 NT-ES cells was narrowed down by FISH analyses with 11 BAC probes located at chromosome 6q. The results demonstrated that the BAC clone RP23-330K23 (located at 6qD3) spanned the 6q breakpoint of T(1;6) (fig. 5).

Normal Differentiation Potentials of N-ntES Cells with Karyotypic Changes

All ES cells examined were positive for alkaline phosphatase activity (fig. 6A) and Oct-3/4 immunoreactivity (data not shown), indicating that the ntES cells were in an undifferentiated state. ES cells treated with retinoic acid and cultured without LIF or feeder cells differentiated into ectoderm, neurons, mesodermal fibroblast-like cells, and parietal endoderm-like cells (fig. 6B). The morphological observations were verified by indirect immunofluorescence using the ectodermal neuronal markers NeuN and GAD67 (fig. 6C, D) and the mesodermal marker desmin (fig. 6E).

The differentiation potentials of the ntES cells were characterized by means of RT-PCR analyses. The *Pou5f1* gene was expressed in all undifferentiated ES cells. Differentiated EB cells, induced by retinoic acid, expressed several somatic cell-lineage marker genes: *Afp* and *Ttr* genes as endoderm markers; *Myh6* as a mesoderm marker; and *Gfap*, *Gria1*, and *Gabrb1* as ectoderm markers (fig. 6F). N-ntES cells and TT2 ES cells were injected separately into the flanks of nude mice to monitor the devel-

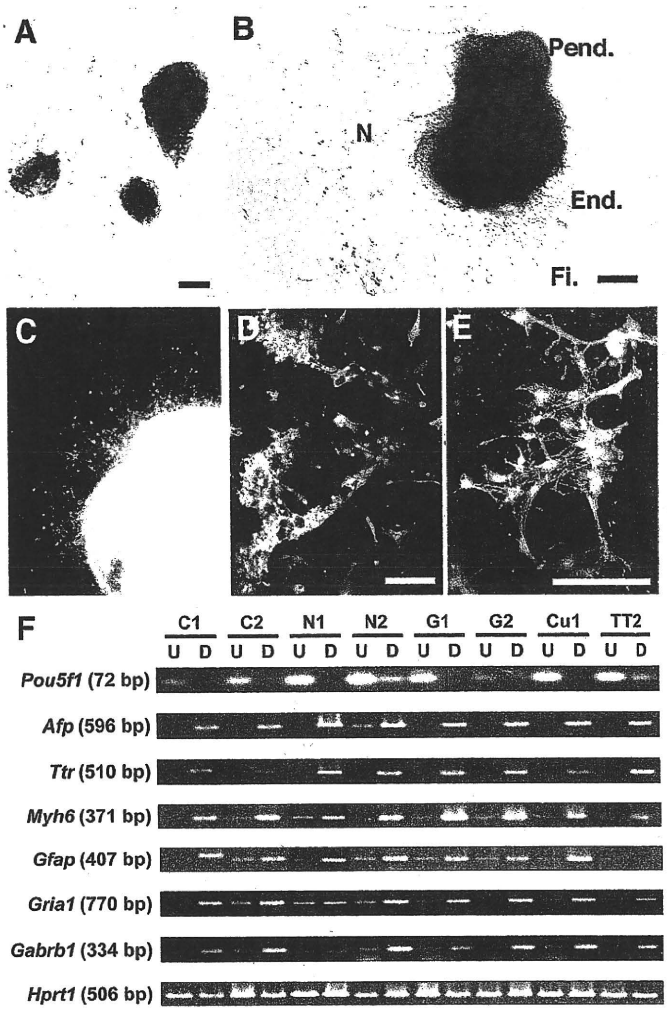

Fig. 6. Differentiation of ES cells derived from neuronal cell nuclei in vitro. **A** Alkaline phosphatase activity was detected in ES cell colonies (brown) but not in feeder cells. **B** Gross morphology of the Cam-1 ES cells differentiated in vitro. A variety of cell types was observed, including neuronal (N, ectoderm), fibroblast-like (Fi, mesoderm), endothelial-like (End., endoderm) and parietal endoderm-like (Pend.) cells. **C–E** Neuronal induction of the ES cells in vitro by retinoic acid. Permanent genetic marking was achieved by GFP expression in the Cam-1 (**C**, **D**) and Cam-2 (**E**) lines. Indirect immunofluorescence revealed neuronal ectodermal derivatives stained with antibodies to GAD67 (**C**) and NeuN (**D**), and mesodermal mesenchymal cells reactive to the anti-desmin antibody (**E**). Scale bars = 50 μm. **F** RT-PCR analyses of marker gene expressions in undifferentiated (U) ES cells and differentiated (D) EB cells. The ES cells were cultured for 3 days on feeder cells with LIF, and the EB cells for 8 days without feeder cells or LIF.

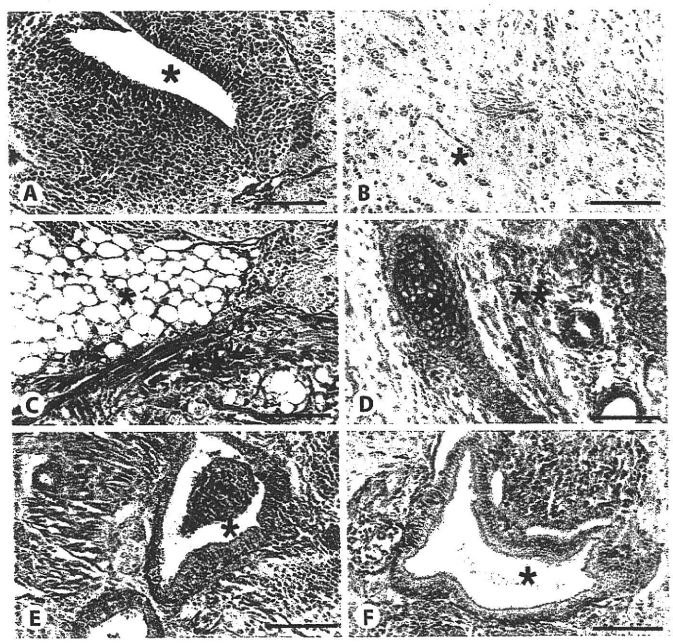

Fig. 7. NtES cell differentiation in vivo. Histological examination by means of hematoxylin and eosin staining (**A**, **C**, **E**) and staining with the antibody to GAD67 of teratocarcinomas resulting from Cam-2 injection (**B**, **D**, **F**). Sections show the presence of ectoderm, i.e., neural epithelium (asterisks in **A**, **B**), mesoderm, i.e., fatty tissue (single asterisk in **C**), cartilage (single asterisk in **D**), and muscle (double asterisks in **C**, **D**), and endoderm, i.e., ciliated epithelium (asterisks in **E**, **F**). Bars = 100 μm.

opment of teratocarcinomas in vivo. 3–5 weeks after the injections, with the exception of Nex-2, all ntES cells and the TT2 ES cells had given rise to tumors. Histological examination showed that the teratocarcinomas from each ES cell were composed of all 3 embryonic germ layers; that is, neural epithelium (ectoderm), muscle and cartilage (mesoderm), and the ciliated epithelium (endoderm) (fig. 7A–F).

Discussion

We previously described our use of NT to study the chromosomal constitution of the nuclei from postmitotic neurons [Osada et al., 2002]. Our findings were consistent with the observation of chromosomal variations in the developing and adult brain [Rehen et al., 2002]. However, since the detection of any genetic changes in the nervous system is currently technically challenging [Chun, 2004], we need more accurate methods for the assessment of the chromosomal properties of neurons. To achieve this objective, in the present study we analyzed the chromosomes of neuron-injected NT embryos at 3 developmental stages (fig. 1).

The SKY method was used to detect balanced and unbalanced chromosomal translocations in metaphase spreads as well as to determine more accurately the number of chromosomes that were gained or lost than can be attained with conventional G-banding in the mouse. First, we examined the chromosomal constitution of N-ntES cells, which were presumably derived from single N-NT embryos, and found chromosomal rearrangements in all Nex-2 N-ntES cells examined. These N-ntES cells with translocations did not form tumors, although in vitro differentiation revealed the expression of several differentiation marker genes in the Nex-2-derived EB cells. We therefore speculate that the translocation may have a suppressive effect on tumorigenesis in vivo.

Determination of whether ntES cells are established from embryos with aneuploidy, which has been reported to occur in neural subpopulations, is of interest [Rehen et al., 2001; Kingsbury et al., 2005]. It is also important to establish whether the chromosomal rearrangements in the N-ntES cells reflect genomic changes that normally occur in the nervous system, or if they are de novo mutations generated during the experimental protocol. We observed that only a minor subpopulation of the N-ntES cells possessed chromosomal rearrangements, suggesting that the karyotypic changes were generated during the experimental processes. We further analyzed the chromosomal constitution of the N-NT embryos in the earlier developmental stages. First, we re-examined the chromosome spreads of the N-NT and C-NT embryos during the first mitotic cleavage. Aneuploidy was detected in the mitotic spreads from N-NT and C-NT embryos, but no specific aneuploid chromosomes were observed. Moreover, the difference in the frequency of aneuploidy between the N-NT and C-NT embryos during the first mitotic cleavage was not statistically significant.

The SKY analyses yielded other cytogenetic information, including findings related to translocation events. Both balanced and unbalanced translocations were detected in the N-NT embryos. Since the translocation patterns were diverse, it was not clear whether the chromosomal changes were innately generated in the donor cell nuclei. To examine this issue further, we assessed premature chromosome condensation (PCC) figures, which form within 2–3 h after injection of exogenous DNA into the ooplasm. We detected aneuploidy, fragmented chromatids, and undercondensed chromatids, which were also detected during the first mitotic cleavage in our previous study [Osada et al., 2002]. DNA damage may lead to inappropriate chromatid condensation in the ooplasm because a lack of DNA repair enzymes can induce aberrant condensation of chromosomes at metaphase [Hittelman et al., 1974; Deckbar et al., 2007].

The causes of translocation in the condensed chromatids in neuron-injected oocytes are largely unknown. One possibility is that the translocation is innately generated in the donor nucleus. Such a translocation would change the global nuclear architecture of the neuronal genome, which may then define the gene expression profiles that support neuronal functions. However, no evidence of DNA recombination in the nervous system has been found so far. Another possibility is that instability of the chromosomes in ES cells [Humpherys et al., 2001] results in translocation. The translocations detected in our study may have been generated during the transformation into ES cells. However, the translocations observed in the NT embryos, especially in the condensed chromatids of the NT oocytes, could not have resulted from such an event.

Another possibility is that the DNA repair machinery in the ooplasm is activated when the neuronal DNA is exposed to the oocyte cytoplasm. DNA repair-associated proteins are expressed and function in oocytes [Ashwood-Smith and Edwards, 1996; Kuznetzov et al., 2007], and evidence has been presented that mutations occur in neuronal DNA in association with aging [Lu et al., 2004; Gonitel et al., 2008]. It is possible that double-strand

eaks (DSBs) in the neuronal DNA can be repaired in ›cytes within a short period of time as a result of non-›mologous end joining. In this case, translocation would :cur in non-specific DNA sequences, many of which ›uld have no apparent effect on cell differentiation or ıysiology. However, our data revealed defects in the dif-rentiation potentials of the NT-ES cells (Nex-2) in vivo ıat exhibited clonally balanced translocations. In addi-›n, it has been shown recently that DSBs in DNA medi-ed by topoisomerase II are generated at transcription-ly active loci [Ju et al., 2006], while we found that the AC clone RP23-330K23 spanned the 6q breakpoint of (1;6) in the Nex-2 NT-ES cells. Since the entire region f the BAC clone RP23-330K23 is contained within the *am19a1* gene, the 6q breakpoint of T(1;6) was also ıapped within the *Fam19a1* gene. The function of the *am19a1* gene product is not known but its expression is estricted to the brain [Tom Tang et al., 2006]. We specu-ıte that the observed chromosomal translocation in the Nex-2 NT-ES cells occurred at a gene locus where dsDNA ›reak-mediated transcription was actively taking place.

Previous studies have demonstrated that chromosom-ıl breaks, observed as the fragmentation of chromo-›omes, may be a cause of the developmental inefficacy of NT-embryos [Wakayama et al., 2000]. The SKY analysis we used in the present study enabled us to visualize un-›alanced and balanced chromosomal translocations and :o identify the chromosomal alterations. Although our data showed that aneuploid or fragmented chromosomes were more common, translocations in the DNA of the N-NT embryos were also detected. Since we did not detect translocations in the C-NT DNA, such changes may be specific for N-NT embryos, not for NT embryos in gen-eral, and are therefore possibly responsible for the ob-served inefficient developmental rate of the N-NT em-bryos [Osada et al., 2005].

To summarize, we examined the chromosomal con-stitution of oocytes injected with DNA from postmitotic neurons and their derivative ntES cells. Translocations were detected in the ntES cells derived from N-NT em-bryos and in the NT embryos during PCC formation and the first mitotic cleavage. Our findings indicate that some donor neurons may exhibit chromosomal changes that restrict the developmental potential of the neuronal ge-nome. We also detected frequent chromosomal changes during the first cleavage of N-NT embryos. These find-ings raise the possibility that DNA repair systems acti-vated in the ooplasm may cause accidental chromosomal rearrangements. Although the ontology of the chromo-somal rearrangements in N-NT oocytes is still unclear, our data provide new evidence for the genetic/epigenetic regulation of neuronal genomes through a unique bio-logical window.

Somatic reprogramming can currently be achieved by means of induced pluripotent stem (iPS) cell technology [Takahashi et al., 2006]. The creation of a massive collec-tion of neuron-derived monoclonal cell lines as a source for abundant DNA from individual neurons would create a valuable resource for investigators in this field. Since the re-entry of neurons into the cell cycle causes apoptosis in neurodegenerative diseases [Kruman et al., 2004], the data from genetic studies of neuronal DNA may reveal ways to protect neurons from degeneration, in particular by clarifying which reprogramming factors regulate the ability of postmitotic neurons to proliferate. In combina-tion with high-performance sequencing technology [Eid et al., 2009], single neuron-based whole-genome sequenc-ing can be expected to provide definitive evidence for ge-netic contributions to the complexity and specificity of individual neurons.

Acknowledgements

We thank Mr. Jan K. Visscher for proofreading and editing of the manuscript and Dr. Hirokazu Kusakabe for informative in-sight into cytogenetic analyses of early embryos.

This study was supported in part by grant-in-aid from the Ministry of Education, Science, Sports, and Culture of Japan (T.O., N.K., and T.Y.), the CREST (Core Research for Evolutional Science and Technology) of JST (Japan Science and Technology Agency) (Y.T.), and a COE (Center of Excellence) funding pro-gram of Osaka University (T.O.).

References

Albert B, Johnson A, Lewis J, Raff M, Roberts K, Walter P (eds): Cancer, in: Molecular Biology of the Cell, 4th ed, pp 1187–1216 (Garland Science, New York 2002).

Ashwood-Smith MJ, Edwards RG: DNA repair by oocytes. Mol Hum Reprod 2:46–51 (1996).

Bain G, Kitchens D, Yao M, Huettner JE, Gottlieb DI: Embryonic stem cells express neuronal properties in vitro. Dev Biol 168:342–357 (1995).

Chun J: Choice, choice, choice. Nat Neurosci 7: 323–325 (2004).

Chun JJ, Schatz DG, Oettinger MA, Jaenisch R, Baltimore D: The recombination activating gene-1 (RAG-1) transcript is present in the murine central nervous system. Cell 64:189–200 (1991).

Deckbar D, Birrauz J, Krempler A, Tchouandong L, Beucher A, et al: Chromosome breakage after G2 checkpoint release. J Cell Biol 176: 749–755 (2007).

Eid J, Fehr A, Gray J, Luong K, Lyle J, et al: Real-time DNA sequencing from single polymerase molecules. Science 323:133–138 (2009).
Gonitel R, Moffitt H, Sathasivam K, Woodman B, Detloff PJ, et al: DNA instability in post-mitotic neurons. Proc Natl Acad Sci USA 105:3467–3472 (2008).
Gossen JA, de Leeuw WJ, Tan CH, Zwarthoff EC, Berends F, et al: Efficient rescue of integrated shuttle vectors from transgenic mice: a model for studying mutations in vivo. Proc Natl Acad Sci USA 86:7971–7975 (1989).
Hittelman WN, Rao PN: Premature chromosome condensation. I. Visualization of x-ray-induced chromosome damage in interphase cells. Mutat Res 23:251–158 (1974).
Hogan B, Beddington R, Constantini F, Lacy E (eds): Isolation, culture, and manipulation of embryonic stem cells, in: Manipulating the Mouse Embryo; a Laboratory Manual, 2nd ed, pp 253–290 (Cold Spring Harbor Press, New York 1994).
Humpherys D, Eggan K, Akutsu H, Hochedlinger K, Rideout WM 3rd, et al: Epigenetic instability in ES cells and cloned mice. Science 293:95–97 (2001).
Johnson FB, Sinclair DA, Guarente L: Molecular biology of aging. Cell 96:291–302 (1999).
Ju BG, Lunyak VV, Perissi V, Garcia-Bassets I, Rose DW, et al: A topoisomerase IIbeta-mediated dsDNA break required for regulated transcription. Science 312:1798–1802 (2006).
Kakazu N, Taniwaki M, Horiike S, Nishida K, Tatekawa T, et al: Combined spectral karyotyping and DAPI banding analysis of chromosome abnormalities in myelodysplastic syndrome. Genes Chromosomes Cancer 26: 336–345 (1999).
Kingsbury MA, Friedman B, McConnell MJ, Rehen SK, Yang AH, et al: Aneuploid neurons are functionally active and integrated into brain circuitry. Proc Natl Acad Sci USA 102: 6143–6147 (2005).
Kruman II, Wersto RP, Cardozo-Pelaez F, Smilenov L, Chan SL, et al: Cell cycle activation linked to neuronal cell death initiated by DNA damage. Neuron 41:549–561 (2004).
Kuznetzov S, Pellegrini M, Shuda K, Fernandez-Capetillo O, Liu Y, et al: RAD51C deficiency in mice results in early prophase I arrest in males and sister chromatid separation at metaphase II in females. J Cell Biol 176:581–592 (2007).
Lee JD, Kamiguchi Y, Yanagimachi R: Analysis of chromosome constitution of human spermatozoa with normal and aberrant head morphologies after injection into mouse oocytes. Hum Reprod 9:1941–1946 (1996).
Liyanage M, Coleman A, du Manoir S, Veldman T, McCormack S, et al: Multicolour spectral karyotyping of mouse chromosomes. Nat Genet 14:312–315 (1996).
Lu T, Pan Y, Kao SY, Li C, Kohane I, et al: Gene regulation and DNA damage in the aging human brain. Nature 429:883–891 (2004).
Mattick JS, Mehler MF: RNA editing, DNA recoding and the evolution of human cognition. Trends Neurosci 31:227–233 (2008).
Mikamo K, Kamiguchi Y: A new assessment system for chromosomal mutagenicity using oocytes and early zygotes of the Chinese hamster, in Ishihara T, Sasaki MS (eds): Radiation-Induced Chromosome Damage in Man, pp 411–432 (Alan R. Liss, New York 1983).
Muotri AR, Chu VT, Marchetto MC, Deng W, Moran JV, Gage FH: Somatic mosaicism in neuronal precursor cells mediated by L1 retrotransposition. Nature 435: 903–910 (2005).
Osada T, Kusakabe H, Akutsu H, Yagi T, Yanagimachi R: Adult murine neurons: their chromatin and chromosome changes and failure to support embryonic development as revealed by nuclear transfer. Cytogenet Genome Res 97:7–12 (2002).
Osada T, Tamamaki N, Song SY, Kakazu N, Yamazaki Y, et al: Developmental pluripotency of the nuclei of neurons in the cerebral cortex of juvenile mice. J Neurosci 25:8368–8374 (2005).
Redon R, Ishikawa S, Fitch KR, Feuk L, Perry GH, et al: Global variation in copy number in the human genome. Nature 444:444–454 (2006).
Rehen SK, McConnell MJ, Kaushal D, Kingsbury MA, Yang AH, Chun J: Chromosomal variation in neurons of the developing and adult mammalian nervous system. Proc Natl Acad Sci USA 98:13361–13366 (2001).
Rudak E, Jacob PA, Yanagimachi R: Direct analysis of the chromosome constitution of human spermatozoa. Nature 274:911–913 (1978).
Takahashi K, Tanabe K, Ohnuki M, Narita M, Ichisaka T, et al: Induction of pluripotent stem cells from adult human fibroblasts by defined factors. Cell 131:861–872 (2006).
Tom Tang Y, Emtage P, Funk WD, Arterburn M, Park EE, Rupp F: TAFA: a novel secreted family with conserved cysteine residues and restricted expression in the brain. Genomics 83:727–734 (2006).
Wakayama T, Tateno H, Mombaerts P, Yanagimachi R: Nuclear transfer into mouse zygotes. Nat Genet 24:108–109 (2000).
Yagi T, Tokunaga T, Furuta Y, Nada S, Yoshida M, et al: A novel ES cell line, TT2, with high germline-differentiating potency. Anal Biochem 214:70–76 (1993).
Ziegler D, Masui Y: Control of chromosome behavior in amphibian oocytes. I. The activity of maturing oocytes including chromosome condensation in transplanted brain nuclei. Dev Biol 35:283–292 (1973).

Experimental and Molecular Pathology 88 (2010) 90–95

Contents lists available at ScienceDirect

Experimental and Molecular Pathology

journal homepage: www.elsevier.com/locate/yexmp

RhoB enhances migration and MMP1 expression of prostate cancer DU145

Misao Yoneda [a], Yoshifumi S. Hirokawa [b,*], Atsuyuki Ohashi [b], Katsunori Uchida [b], Daisuke Kami [c], Masatoshi Watanabe [c], Toyoharu Yokoi [a], Taizo Shiraishi [b], Shinya Wakusawa [a]

[a] Department of Medical Technology, Nagoya University School of Health Sciences, 1-1-20 Minami, Daiko, Higashi-ku, Nagoya City, Aichi, Japan
[b] Department of Pathologic Oncology, Institute of Molecular and Experimental Medicine, Faculty of Medicine, Mie University Graduate School of Medicine, 2-174 Edobashi, Tsu, Mie 514-8507, Japan
[c] Laboratory for Medical Engineering, Division of Materials Science and Chemical Engineering, Graduate School of Engineering, Yokohama National University, Japan

ARTICLE INFO

Article history:
Received 27 March 2009
and in revised form 15 September 2009
Available online 24 September 2009

Keywords:
RhoB
GSK-3
MMP1
Prostate cancer

ABSTRACT

Rho family protein regulates variety of cellular functions as cytoskeletal organization, cell proliferation and apoptosis. In the present study, we demonstrate that RhoB-overexpressed prostate cancer cells showed an enhanced cell motility and the administration of the GSK-3 inhibitors inhibited this increase in migration. Among the extracellular matrix and adhesion-related molecules, MMP1 RNA expression was increased in RhoB-overexpressed cells, administration of MMP inhibitor suppressed the collagen gel invasion in these cells. This is the first report evaluating RhoB function and the downstream signaling events in prostate cancer cell. Our results indicate that RhoB promotes cell motility and invasion in a metastatic prostate cancer cell.

Introduction

Rho GTPase, RhoA, RhoB and RhoC regulate the organization of the cytoskeleton and cell motility (Wheeler and Ridley 2004). Among the Rho family of proteins, particular attention has been focused on RhoA, Rac1 and Cdc 42 since these molecules play central roles in cell migration through the regulation and formation of actin stress fiber, filopodia and lamellipodia, respectively (Ridley and Hall, 1992; Ridley et al., 1992; Kozma et al., 1995). The relevance of the subcellular RhoB localization at the endosome (Adamson et al., 1992), an RhoB function, is proposed to regulate membrane trafficking such as EGF receptor (Wherlock et al., 2004) and Src (Sandilands et al., 2004). In addition to its GTPase status, RhoB function is also influenced by the C terminal prenylated modification of either farnesylation or geranylgeranylation in apoptotic response, mitosis, tumor growth and actin organization (Liu et al., 2000; Moasser et al., 1998; Chen et al., 2000; Allal et al. 2002). The RhoB protein is induced by a variety of stimuli in vitro, including UV irradiation, cytokines and growth factors (Prendergast 2001). In vitro cancer model, RhoB overexpression, inhibits migration and invasion. RhoB suppresses melanoma metastasis in mouse xenograft model (Jiang et al., 2004). On the contrary, fibroblasts from RhoB knockout mice migrate less than the wild-type counterpart (Liu et al., 2001).

Processing and or degrading varieties of substrates in extracellular milieu, the matrix metalloproteinases (MMPs) play central roles in tissue remodeling, promoting cancer invasion and metastasis (Sternlicht and Werb 2001). MMP1 is associated with a poor prognosis of colon cancer (Murray et al., 1996), involved in the invasive potential of lung cancer (Schütz et al., 2002). The genetic variants of MMP1, that lead to a high protein expression, are epidemiologically linked with ovarian cancer, metastatic melanoma and lung cancer (Sternlicht and Werb 2001; Sauter et al., 2008).

In preliminary experiments, when a prostate cancer cell line DU145 was treated with reagents that promoted DNA demethylation and chromatin acetylation, RhoB RNA expression was stimulated to about ninety times the level of the untreated cells. Treating the same reagents of another prostate cancer cell line LNCap, RhoB expression was enhanced only about two times. Here we generated DU145 cell lines stably expressing RhoB and examined the effect of RhoB on cellular motility and invasion.

Materials and methods

Cell lines and reagents

The human RhoB cDNA was PCR amplified from the Clone Collection (Open Biosystems, EHS1001-7571211) and subcloned into the pcDNA3-HA vector. After introduction of the vector with or without the insert into the prostate cancer DU145 cell line, G418-selected clones were isolated. Up-regulation of the RhoB RNA/protein in these cells was confirmed. The SCADS inhibitor kit was generously supplied from Screening Committee of Anticancer Drugs supported by a Grant-in-Aid for Scientific Research on Priority Area "Cancer" from The Ministry of Education, Culture, Sports, Science and Technology, Japan. Two GSK-3 inhibitors, GSK-3 inhibitor IX (CalbioChem, 361550) and Indirubin-3′-monoxime-5-sulphonic acid (CalbioChem, 402085), were added to the culture at a final concentration of 10 μM.

* Corresponding author. Fax: +81 59 231 5210.
E-mail address: ultray2k@clin.medic.mie-u.ac.jp (Y.S. Hirokawa).

0014-4800/$ – see front matter © 2009 Elsevier Inc. All rights reserved.
doi:10.1016/j.yexmp.2009.09.010

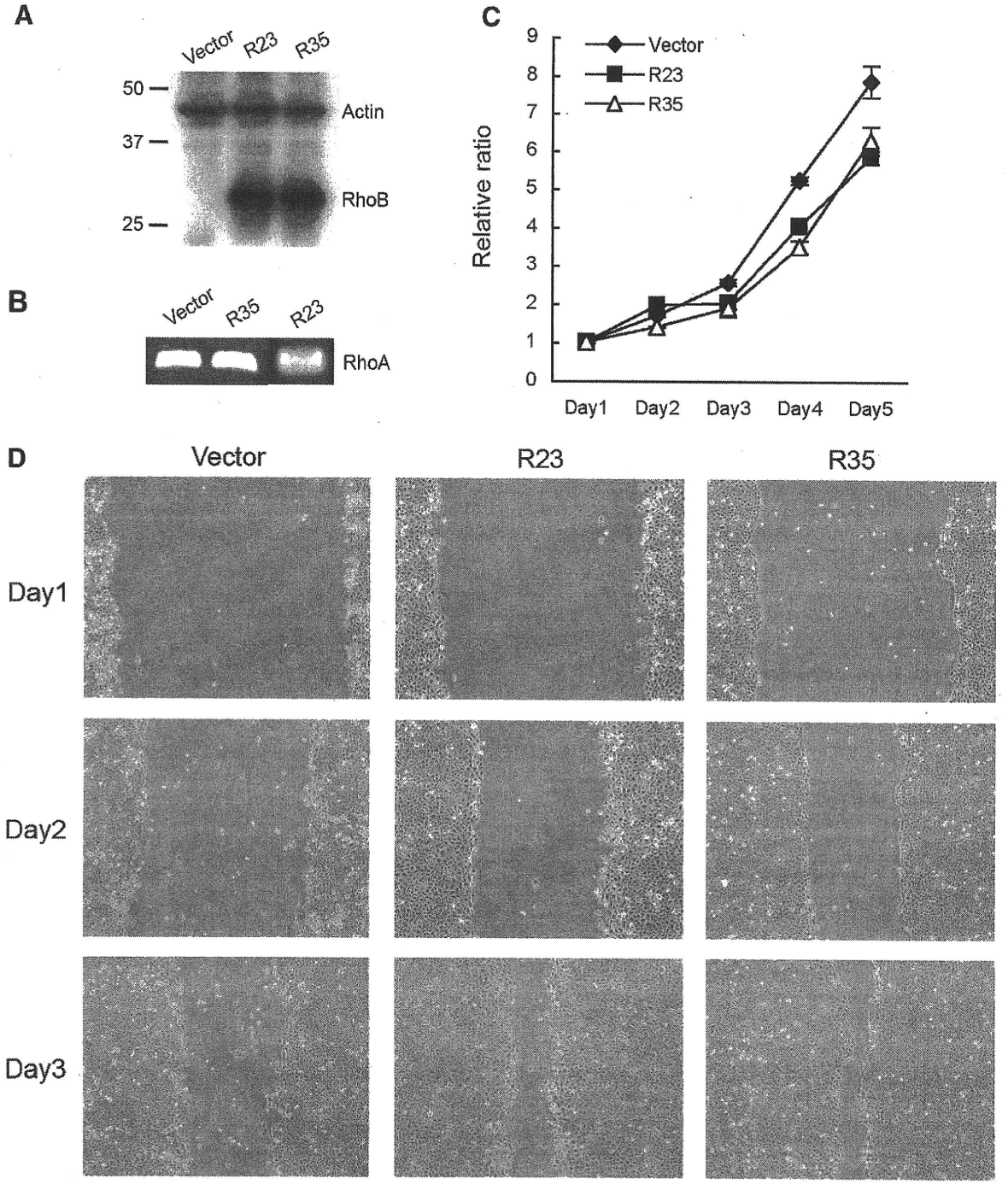

Fig. 1. RhoB overexpression promotes the migration of prostate cancer cells. (A) Western blot detection of two RhoB stably expressed clones R23 and R35 next to the vector-only-transfected clone. (B) RhoA mRNA expression levels in vector, R35 and R23 clone. (C) Cell growth up to 5 days culture are plotted as relative ratio to day 1. Data shown are mean ± SD of triplicates, representation from three independent experiments. (D) Wound closure assay with vector, R23 and R35 clones. Migration of each cell was observed for 3 days after the cells were scraped off. Images are representative of three independent experiments.

Wound closure/cell migration assays

The cells were cultured in RPMI 1640 (Sigma, R8758) with 10% fetal bovine serum (Gibco/Invitrogen) and seeded to a confluent density in 6 cm tissue culture dishes. For the wound closure assay, the monolayer of cells was scraped with the edge of a Cell Scraper (Iwaki, 9000-220). The cell migration assay was performed using the Boyden chamber method. Briefly, the cells were labeled with fluorescence Dil (Molecular Probes, D383) at 20 μg/ml in 6-cm tissue culture dishes for 6 h. Dil was dissolved in DMSO initially and then diluted in 100% EtOH. Dil-labeled 10^5 cells in 100-μl medium without FBS were loaded in the upper chamber (Falcon, 353097); the reagents from SCADS inhibitor kit and GSK-3 inhibitors were added to the bottom wells. After an overnight incubation, unmigrated cells were removed with a cotton swab, the chambers were placed in a new empty plate and the fluorescence of migrated cells was measured from the bottom direction using a plate reader.

The cell viability after administration of GSK-3 inhibitors was measured using the MTT assay according to the manufacturer's instructions (Promega, G3580). Each experiment was repeated at least twice in triplicate except for the SCADS inhibitor assay which was performed once because of the limited amount of the reagents.

eal-time PCR

Total RNA was isolated from prostate cancer cell lines using an NA extraction kit according to the manufacturer's protocol (QIAGEN, 4104). First-strand cDNA synthesis was performed using the uperscript II RNase Reverse Transcriptase kit (Invitrogen, 18080-44). The expression of 84 genes of the human extracellular matrix nd adhesion molecules was analyzed according to the instructions of he RT^{2}Profiler PCR Array (SuperArray, PAHS-013A).

The primer sequences of RhoA were forward, 5′ TTACTCCGTAACA-GATTTTGTTGGC 3′, and reverse, 5′ ATACTACATCTAGTCTGGGGTAGAT 3′.

Collagen type I gel invasion assay

Invasion assays were carried out with a Cultrex 24-well collagen cell invasion assay kit (3457-024-K) directed as the manufacture's nstruction with a modification. Briefly, cells were cultured at 5×10^5 number in 6-cm plate, on the next day, 5×10^4 cells were suspended in 98 μl of RPMI 1640 with 0.5% fetal bovine serum, adding 2 μl of 5× collagen I solution, after mixing with pipeting, a 100-μl of cell/collagen mixed solution was aliquoted in each chamber (Falcon, 353097). Bottom well was loaded RPMI 1640 with 10% fetal bovine serum. After an overnight incubation, uninvaded cells were removed with a cotton swab, the chambers were placed back to the original wells with cell counting assay reagent (Cell Counting Kit-8, DOJINDO) and the absorbance of invaded cells was measured using a plate reader. Evaluating the MMP1 function of RhoB-overexpressed cells, MMP inhibitor II (CALBIOCHEM, #444247) was added to the medium of 6-cm plate at 100 μM and the cells were incubated for 6 h before the collagen gel chamber assay.

Both experiments were repeated three times in triplicate.

Results

RhoB overexpression enhanced prostate cancer cell migration

Two of the clones, designated R23 and R35, showed high RhoB protein expression compared to the vector-transfected clone (Fig. 1A). The proliferation rate at the culture conditions was slightly slower in R25 and R35 than vector-transfected cells, but this difference was not robust for the first three days (Fig. 1C). On culture days 4 and 5, vector-transfected cells grew faster than R25 and R35. Since RhoA also plays a pivotal role in cell proliferation, adhesion and migration, evaluating the RhoA status in prostate cancer cell migration under the test conditions was essential. The mRNA expression levels of RhoA were found to be similar in vector, R35 and R23 clone (Fig. 1B). When the migration rates were compared using the "wound closure assay", R23 and R35 showed faster movement than the vector clone in covering the "cellular defect" on the bottom of the scraped dish (Fig. 1D). This result clearly suggested the overexpression of the RhoB protein enhanced prostate cancer cell migration.

GSK-3 inhibitor suppressed migration of RhoB-expressed prostate cancer cells

In order to determine the signal mechanism underling the enhanced migration due to overexpression of the RhoB protein, an SCADS inhibitor kit was used for the migration assay. This kit includes several types of inhibitors commercially available. As described in the Materials and methods section, the initial cell migration was assessed by the Boyden chamber assay. Among the inhibitors inducing migratory suppression, GSK-3 inhibitors were chosen for the second round analysis. In cells treated with DMSO (vehicle), cell motility of R23 and R35 clones was twice that of the vector clone (Figs. 2A and B). Two of the GSK-3 inhibitors, GSK-3 inhibitor IX and Indirubin-3′-monoxime-5-sulphonic Acid, reduced the migration of R23 and R35 clones at the same level as that of the vector clone (Figs. 2A and B). Since the cell motility suppression was observed in the vector clone, GSK-3 inhibitors seemed to suppress endogenous RhoB effect as well. The cell viability of the three clones after treatment with GSK-3 inhibitors was not significantly different from each other (Fig. 2C).

Increased expression of MMP1 in RhoB-expressed prostate cancer and enhanced collagen gel invasion

Since cellular movement is closely associated with cell attachment, the mRNA levels of extracellular matrix and adhesion molecules were measured using real-time PCR (RT^{2}Profiler PCR Array). The most of gene expression levels were similar between R35 and vector clone (Table 1). The substantial fold changes between R35 versus vector clone were 2.36 of ADAM metallopeptidase with thrombospondin type 1 motif 8, 0.68 of E-cadherin, 0.55 of Vitronectin. Among the gene expression levels that were altered, MMP1 expression was about five times higher in the R35 clone than in the vector clone. The major substrates of MMP1 are collagens I, II and III. Verifying the functional relevance of MMP1 expression in the RhoB-overexpressed clones, chamber invasion assay was performed with type I collagen gel, which is the ubiquitously distributed interstitial matrix. Both R23 and R35 clones invaded through collagen gel more than vector clone (Fig. 3A). Prior to the chamber assay, incubating these cells with MMP inhibitor II, an inhibitor of MMP1, 3, 7 and 9, suppressed these enhanced cell invasion (Fig. 3B). These results indicate that MMP1 induction in RhoB-overexpressed prostate cancer cell is one of the mechanisms of increased migratory and invasive behavior of these cells.

Discussion

In the current study, we showed that the overexpression of RhoB enhanced cellular movement and invasion of prostate cancer cells in vitro. Increased motility is mediated by GSK-3 signaling and invasive potency is dependent on MMP1.

Previously, RhoB was shown to suppress the migration of NIH3T3 cells, invasion of pancreatic cancer cells and lung metastasis of melanoma cells (Jiang et al., 2004). RhoB-null macrophages also migrated faster on fibronectin (Wheeler and Ridley 2007). On the contrary, embryonic fibroblasts from an RhoB-null mouse showed less motility than wild-type fibroblasts in a wound closure test (Liu et al., 2001). Although the migratory mechanisms involved in these reverse functions of RhoB have not been fully elucidated yet, RhoB could play opposite roles within different cellular contexts. In NIH3T3 cells, GTPase-active and farnesylated RhoB can maintain an organized actin cytoskeleton and stress fibers against geranylgeranyl transferase inhibitor, which disrupts the actin cytoskeletal network (Allal et al., 2002). In this manner, the RhoB status of GTPase and prenylation could be different in each cellular type, consequently influencing actin fiber organization and cellular motility.

Fig. 2. GSK-3 inhibitors suppress motility of each cell clone in the chamber mobility assay. (A) Fluorescence microscope images of chamber membranes. Cells were plated inside the chamber in serum-free medium and allowed to migrate to serum and inhibitor-containing medium at the bottom for 12 h. (B) Migrated cell numbers were assessed in terms of the fluorescence value of each chamber. Data shown are mean ± SD of triplicates, representation from three independent experiments. (C) Cell viability of each clone was measured using the MTT assay after treatment of cells with GSK-3 inhibitors. Data shown are mean ± SD of triplicates, representation from two independent experiments.